Earth-Science Reviews 224 (2022) 103884

Contents lists available at ScienceDirect

Earth-Science Reviews

journal homepage: www.elsevier.com/locate/earscirev

Thermal regime of sedimentary basins in the Tarim, Upper Yangtze and North China Cratons, China

Nansheng Qiu [a,b,*], Jian Chang [a,b], Chuanqing Zhu [a,b], Wen Liu [a,b], Yinhui Zuo [a,c], Wei Xu [a,d], Dan Li [a,b]

[a] State Key Laboratory of Petroleum Resources and Prospecting, China University of Petroleum, Beijing 102249, China
[b] College of Geosciences, China University of Petroleum, Beijing 102249, China
[c] College of Energy Resources, Chengdu University of Technology, Chengdu 610059, China
[d] Department of Earth and Environmental Science, Xi'an Jiaotong University, Xi'an 710049, China

ARTICLE INFO

Keywords:
Tarim Craton
Upper Yangtze Craton
North China Craton
Tarim Basin
Bohai Bay Basin
Sichuan Basin
Thermal regime
Thermal history
Heat flow

ABSTRACT

Thermal regime and thermal history are of significant important in basin dynamics and hydrocarbon generation of source rocks. The sedimentary basins in three typical cratons of China, North China Craton (NCC), Yangtze Craton (YC) and Tarim Craton (TC), underwent completely different tectonic background and dynamic mechanism, which resulted in the differentials of their thermal regimes. In this paper, the thermal regimes of the Bohai Bay Basin in the eastern NCC, Tarim Basin in TC, and Sichuan basin in the Upper YC were studied. There has some lower thermal background in the area of western China than eastern side of the NCC. The mean heat flow value of Tarim basin is 42.5 mW/m^2, 53.8 mW/m^2 in the Sichuan basin and 66.7 mW/m^2 in the eastern NCC. And the temperature at 10000 m ultra-depth in the Tarim Basin also shows lower values than that of Sichuan and Bohai Bay basins. The thermal history, modeled from thermal indicators of vitrinite reflectance (R_o), equivalent vitrinite reflectance data (R_{equ}), fission track and (U—Th)/He data of apatite and zircon, evolved differently because of the different tectonic history in these basins. The Tarim basin underwent a cooling history with the heat flow of 55–65 mW/m^2 in the Cambrian decreasing to the present-day of 40–50 mW/m^2. The Meso-Cenozoic thermal history of the Bohai Bay basin experienced four evolutionary stages with two heat flow peaks in the late Early Cretaceous and in the Middle to Late Paleogene, which correspond to the destruction peaks of the eastern NCC and had heat flow values of 82–86 mW/m^2 and 81–88 mW/m^2, respectively. The Sichuan basin was stable with heat flow value of less than 65 mW/m^2 from the Late Sinian to Late Paleozoic, and the heat flow increased rapidly to the peak value (75–100 mW/m^2) at the end of Early Permian by thermal effect of the Emeishan mantle plume. From Mesozoic to present, the heat flow decreased to the present value (60–70 mW/m^2). In addition, the comparation of thermal characteristics of typical cratons around the world, including heat flow, thermal history, lithospheric thermal structure and thermal lithospheric thickness, also have been caried out. The differential thermal histories of Tarim and Sichuan basins resulted in the different thermal evolution of Cambrian source rocks. This study may provide some new geothermal evidence for hydrocarbon generation and phase distribution of oil and gas in the deep and/or ultra-deep basin.

1. Introduction

Thermal regime or thermal background is of significant important to reveal the geodynamic processes of continental lithosphere (Chapman and Pollack, 1975; Lachenbruch and Sass, 1977; Pollack and Chapman, 1977; Vitorello and Pollack, 1980; Sclater et al., 1980; Morgan and Sass, 1984; Furlong and Chapman, 1987; Pollack et al., 1993) and the generation of hydrocarbon from source rocks in sedimentary basins. Geothermal research also plays an important role in continental craton evolution studies (Michaut et al., 2009; Morgan, 1985; Pollack, 1996), and lithosphere thickness and its thinning can be verified by the thermal history of the sedimentary basin (Hu et al., 2007; Qiu et al., 2014, 2016). There are several cratonic basins of Paleozoic to Cenozoic in the continental area of China. They have complicated geological histories and tectonic styles that caused distinct thermal patterns and thermal histories. As a result, these basins have differing stages of source rock

* Corresponding author at: State Key Laboratory of Petroleum Resources and Prospecting, China University of Petroleum, Beijing 102249, China.
E-mail address: qiunsh@cup.edu.cn (N. Qiu).

https://doi.org/10.1016/j.earscirev.2021.103884
Received 17 April 2021; Received in revised form 24 November 2021; Accepted 30 November 2021
Available online 6 December 2021

maturity and different types of hydrocarbon accumulations.

Heat flow data have been increasing in the past decades, and thermal histories have been reconstructed of main petroliferous basins in China in the past 20 years. All these documents provide the possibility for us to review the thermal regime of typical basins in the continental China. At the same time, the Bohai Bay, Sichuan and Tarim basins are important oil and gas producing areas in China, and ultra-deep oil and gas exploration has been paid attention to and made continuous breakthroughs in these basins in recent years (Wang et al., 2015; Qi, 2016; Li et al., 2019; Ma et al., 2020; Guo et al., 2020; Yang et al., 2020). Whether it is the study of hydrocarbon generation in ultra-deep and/or Cambrian-Precambrian source rocks or the study of phase distribution in ultra-deep reservoirs, need the thermal regime data of basins.

The goal of this review is to summarize the characteristics on thermal regime of main cratonic basins in continental area of China. The next section covers heat flow, deep temperature and thermal structure of lithosphere at the present-day followed by the geological settings. Then there is a section on the thermal history of the main cratonic basins, and then section focusing on hydrocarbon generation of main source rocks in these basins and the comparation between typical stable and destabilized cratons in the world. The main significance of this review is to clarify the thermal regime and thermal history of the main cratonic basins in China, and provides key parameters for the formation and evolution of deep and ultra-deep oil and gas in these areas.

2. Geological settings

Continental China is composed of the southeastern part of the Eurasian Plate and north rim of Indian Plate, and bordered by the Pacific Plate to the east (Fig. 1). It is located in one of the most complex tectonic domains in the world, where the Paleo-Asian Ocean, Tethyan and Western Pacific domains met in a triangular framework, and carrying a mosaic of ancient cratonic blocks and orogenic belts built through

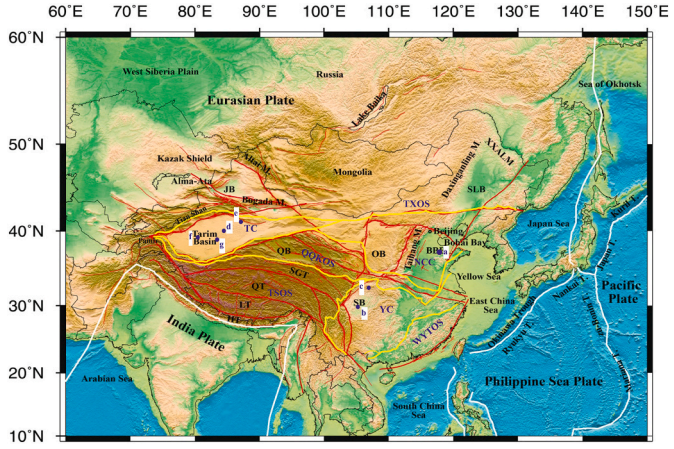

Fig. 1. Topography and tectonic background of China and its surroundings (Modified from Huang and Zhao (2006) and Pan et al. (2009)). Colour shows the surface topography. White curved lines show the plate boundaries. Red lines show the large fault zones and/or tectonic block boundaries in continental China. The yellow lines are tectonic unit boundaries modified from Pan et al. (2009). NCC = North China Craton, QQKOS = Qinling-Qilian-Kunlun Orogenic System, TSOS = Tibet-Sanjiang Orogenic System, TXOS = Tianshan-XingMeng Orogenic System, WYTOS = Wuyi-Yunkai-Taiwan Orogenic System, YC = Yangtz Craton. Blue solid circles show the locations of typical wells in thermal history studies. a. Well Y155, b. Well MX13, c. MS1, d. Well SB5, e. Well KQ1, f. Well HT1, g. Well TZ1. JB = Junggar Basin, QB = Qaidam Basin, SB = Sichuan Basin, OB=Ordos Basin, BBB=Bohai Bay Basin, SLB=Songliao Basin, SGT = Songpan-Ganzi Terrane, QT = Qiangtang Terrane, LT = Lhasa Terrane, HT = Himalaya Terrane, XXAXM = Xiaoxinganling Mountain, M. = Mountain, T. = Trough. (For interpretation of the references to colour in this figure legend, the reader is referred to the web version of this article.)

different tectonic regimes (Zhai and Santosh, 2011; Zheng et al., 2013; Zhao and Zhai, 2013). The fundamental tectonic framework of continental China was finalized in the Early Mesozoic (Huang and Chi, 1980). However, there experienced different tectonic evolutions in the eastern, central and western parts of continental China. Three typical cratons in the continental China, the North China Craton (NCC), Yangtze Craton (YC) and Tarim Craton (TC), developed from the Archean crystalline basement, and they represent the tectonic features of eastern, central and western China (Fig. 1).

2.1. The North China Craton and Bohai Bay Basin

The North China Craton (NCC) has the Archean to Paleoproterozoic crystalline basement, and is overlain by the Mesoproterozoic to Cenozoic sedimentary strata (Zhao and Zhai, 2013). The NCC is composed of the Eastern Block, Western Block and the Central Orogenic Belt (also known as the Trans-North China Orogen) (Zhu et al., 2012; Zhao and Zhai, 2013). The eastern North China Craton (ENCC) experienced two periods of destruction during the Early Cretaceous and Paleogene by evidence from the structural geology, mantle xenoliths, magmatic petrology, magmatic geochemistry, geophysics and geothermics (Chen, 2009; Cheng et al., 2013; Xia et al., 2013; Zhao et al., 2013; Zhu et al., 2012; Qiu et al., 2014, 2015, 2016).

The Bohai Bay Basin is located at the eastern NCC and with an area of approximately 20×10^4 km^2. It is a Meso-Cenozoic rift basin formed on the Archean-Paleoproterozoic crystalline basement. In general, the tectonic history of the basin can be divided into four stages (Tian et al., 2000; Hou et al., 2001; Li, 2003; Xu et al., 2006; Zhang et al., 2009): regional stable deposition (Middle and Late Proterozoic to Paleozoic), fold uplift (early to mid-Mesozoic), *syn*-rift (Early Cretaceous to Paleogene) and regional depression (Neogene to present-day). The Mesozoic was an important tectonic transition period in the Bohai Bay Basin. The basin had previously undergone the Yanshanian Orogeny during the Jurassic to early Cretaceous, characterized by intense tectonic-magmatic activities associated with development of major, lithosphere penetrating faults, including the Tanlu and Taihang faults (Xu et al., 2004a, 2004b; Wu et al., 2005a, 2005b). The Bohai Bay Basin experienced a second phase of rifting in the Paleogene. The basin was filled with Cenozoic lacustrine deposits with a thickness of up to 10,000 m in the deep sags (Fig. 2a). The basin was changed from an extensional environment to a contractional environment in the Neogene, and it was mainly filled with plain-fluvial sediments with a thickness of 1000–3500 m.

2.2. The Yangtze Craton and Sichuan Basin

The Yangtze Craton is a continental block characterized by early growth in the Paleoarchean and subsequent reworking in the Mesoarchean, followed by further growth and reworking in the middle Paleoproterozoic, new crustal additions in the Mesoproterozoic, and intense reworking in the middle Neoproterozoic (Wang and Li, 2001; Zhang and Zheng, 2013). The initial stabilization of the Archean nucleus of the Yangtze Craton occurred between 2.7 and 2.6 Ga (Han et al., 2017). The eastern Yangtze Craton has also been destroyed in the Mesozoic (Lu et al., 2013; Li et al., 2015).

The Sichuan basin is located in the northwest of the Yangtze Craton (also called Upper Yangtze Craton, UYC), with an area of 23×10^4 km^2. The tectonic evolution of the Sichuan Basin included the differential uplift in stretching system from Sinian to the Late Triassic (Z-T_3), the fold-thrust on the background of compression from the Late Triassic to the Eocene (T_3-E), and the uplifting during the folding process from the Oligocene to the present (*E*-Q) (Liu et al., 2014). Several unconformities developed during the tectonic evolution (Fig. 2b). The formations developed in the Sichuan Basin could be divided into two sedimentary systems: the marine carbonate sedimentary from the Sinian to the Middle Triassic and the continental clastic sedimentary from the upper

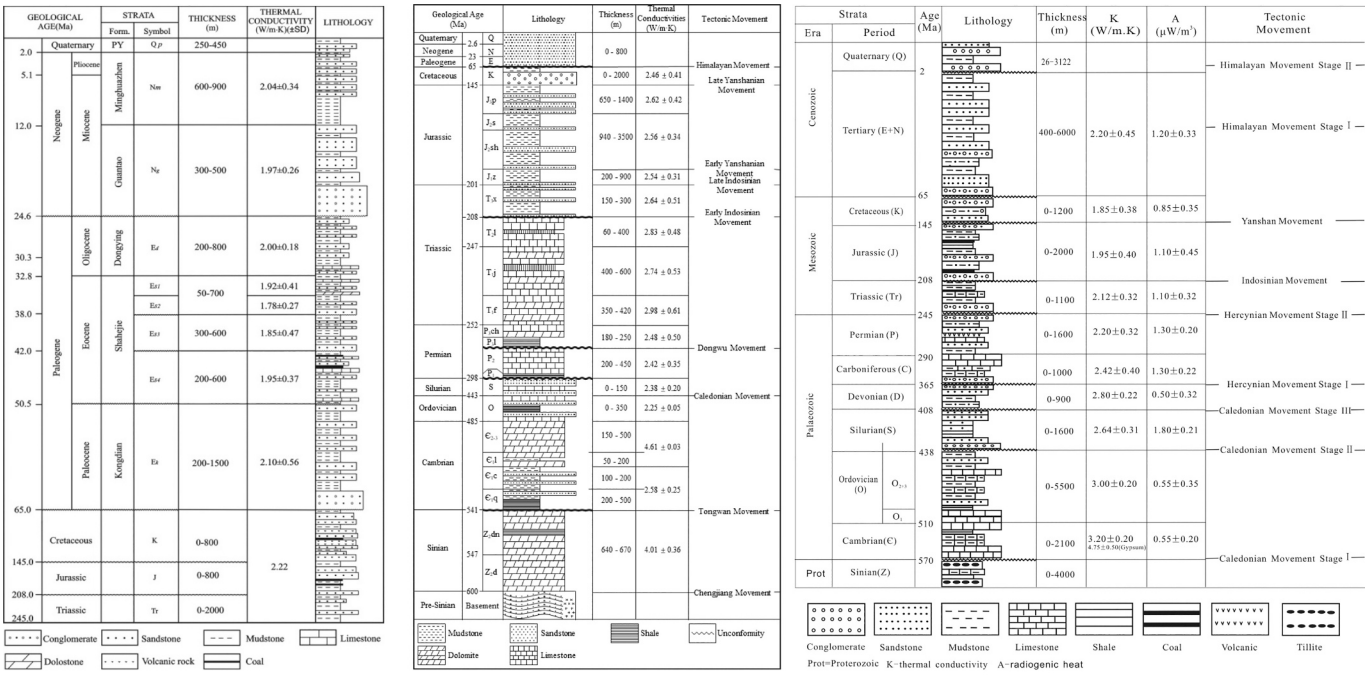

a. Bohai Bay Basin b. Sichuan Basin c. Tarim Basin

Fig. 2. The stratigraphic columnar section of the Tarim basin, Sichuan and Bohai Bay basins.
a. Bohai Bay basin. Thermal conductivity is shown as mean value ± SD from Gong (2003); b. Sichuan Basin. Thermal conductivities data are from references (Li, 1990; Han and Wu,1993; Xu et al., 2011; Tang et al., 2019); c. Tarim Basin. Thermal conductivities and radiogenic heat generation data are from Qiu (2002).

Triassic to the present-day. Several sets of hydrocarbon resource rocks developed in the basin, among which Cambrian Qiongzhusi Formation, Silurian Longmaxi Formation and Permian are the main source rocks and they are currently buried to depths of over 5000 m in most parts of the basin with the stages of high to over mature.

Permian Emeishan large igneous province (ELIP) in SW China is one of the most intensely studied LIPs over the years. Numerous investigations on geochemistry, geochronology, geophysics and paleoenvironment of exposed strata in ELIP have shown that its igneous rocks are likely derived from magmas originated from a mantle plume (e.g., Xu et al., 2004a, 2004b; Ali et al., 2010; Shellnutt, 2014). The province was emplaced at Late Permian (~260 Ma) with a short eruption duration (~1 Ma). Many Permian basaltic rocks were penetrated by deep industrial boreholes in SCB. Recent studies have proposed that these basaltic rocks are temporally associated with the eruption of Emeishan flood basalts (Lu et al., 2019; Ma et al., 2019; Li et al., 2020a, 2020b), indicating that the ELIP may have covered a substantially larger area. Likewise, the thermal history reconstruction displays a significant heat flow perturbation (~100 mW/m^2) at the Late Permian in the basin.

2.3. The Tarim Craton and Tarim Basin

The Tarim Craton, which developed on an Archaean and Proterozoic metamorphosed basement, is located in northwestern China, to the north of the Tibetan Plateau. The Tarim basin is the largest basin in the continental area of China, with an area of 56 × 10^4 km^2. The tectonic evolution of the basin was divided into six stages (Jia et al., 1995): the cratonic peripheral aulacogen from the Sinian to the Ordovician, the intra-cratonic depression from the Silurian to the Early Carboniferous, the intra-cratonic rift from the Late Carboniferous to the Permian, the foreland basin stage in the Triassic, the intra-continental depression from the Jurassic to the Paleogene, and the recombined foreland basin from the Neogene to the Quaternary. Several unconformities developed during the tectonic evolution (Fig. 2c) (Jia et al., 1995; Jia and Wei, 2002; He et al., 2005). The Tarim craton was in a strong extensional state in the Early to Middle Permian and a large number of magmatic rocks were developed in the basin with the distribution area over 25 × 10^4 km^2. Magma from this large igneous province (LIP) erupted at 300–275 Ma (Li et al., 2012 ; Wei et al., 2014; Xu et al., 2014; Yang et al., 2013; Zhang et al., 2013), but large scale basaltic magmatic rocks were formed at 290–288 Ma. The magmatism in this period may affect the thermal state of the basin in the Permian period.

The depositional history of the basin includes marine to non-marine facies during the Sinian to the Early Permian and non-marine facies during the Late Permian to Quaternary (Li et al., 1996; Jia and Wei, 2002). A total thickness of up to 15,000 m of sediments was deposited in the Northern Depression (Huang et al., 1999). There are several hydrocarbon source rocks in the basin, including four sets of marine source rocks in the Cambrian (Є), the Lower Ordovician (O_1), the Middle-Upper Ordovician (O_{2+3}), and the Carboniferous (C), and two terrestrial potential source rocks of Triassic-Jurassic (Tr-J) and Cretaceous-Paleogene (K-E) age. The effective hydrocarbon source rocks in the Tarim basin are mainly the Cambrian carbonate successions and the Middle-Upper Ordovician strata (Zhang et al., 2000, 2001; Zhao et al., 2008; Mu, 2009). They are currently buried to depths of over 5000 m in most areas of the basin, and, as a result, these Lower Paleozoic source rocks are at high mature or over-mature stage (Xiao et al., 2000; Wang et al., 2003a, 2003b).

3. Present-day thermal regime of the basins

Systematic heat flow measurements in the continental area of China were initiated in the 1970s. Since then, a considerable number of heat flow data have been accumulated (Wang and Huang, 1988, 1990; Xiong et al., 1995; Wang et al., 1996a, 1996b; Hu et al., 2000; Jiang et al., 2019). In addition, the heat flow distribution in the sedimentary basins has been extensively studied (Wu and Xie, 1985; Wang and Wang, 1986; Chen, 1988; Wang et al., 1990,Wang et al., 1995a, 1995b; Li, 1992; Wang et al., 1992; Shen et al., 1994). 1230 heat flow data have been published in the continental of China by now (Jiang et al., 2019), and

most heat flow data are from the sedimentary basins. The followings will discuss the characteristics of heat flow, deep-temperature at 10000 m, thermal structure and thermal lithospheric thickness of these three typical cratons/basins.

3.1. Heat flow

The conductive heat transport in the upper crust conforms with the Fourier's law, which states that the heat flow (q) at a point in a medium is directly proportional to the geothermal gradient at the point with the equation:

$$q = -K \bullet \frac{\mathrm{dT}}{\mathrm{dZ}} \tag{1}$$

where, $\frac{dT}{dZ}$ is the geothermal gradient (°C/km); K is the rock thermal conductivity of samples from drilled holes (W/m·K); The negative sign indicates that the direction of the heat flow is opposite to the geothermal gradient.

Rock thermal conductivity is critical parameter for calculating heat flow. For one rock, its thermal conductivity can be expressed as:

$$K = K_m^{1-\varnothing} \times K_w^{\varnothing} \tag{2}$$

where, φis porosity (%), adopting measured porosity or calculated porosity by sonic logging; $K_w{}^{\varnothing}$ is thermal conductivity of fluid filling a hole, adopting 0.6 W/m·K; $K_m{}^{1-\varnothing}$ is thermal conductivity of rock frame (W/m·K) and can be calculated by the following equation:

$$K_{m0} = K_m^{1-\varnothing} \times K_{air}^{\varnothing} \tag{3}$$

where, K_{m0} is measured thermal conductivity for rock samples at room temperature (W/m·K);$K_{air}{}^{\varnothing}$ is thermal conductivity of air, adopting 0.0257 W/m·K. According to the Eqs. (2) and (3), we calculated the in-situ rock thermal conductivity of the dry rock samples. In the following study, most heat flow data are from the data published by others before. Usually, the thermal conductivity should be from drill holes in the measured heat flow data in the sedimentary basins.

Studies of the present-day thermal gradients and heat flow of the Tarim basin have been carried out since the 1990s (Wang et al., 1995a, 1995b; Wang et al., 1996a, 1996b; Wang et al., 2003a, 2003b; Wang et al., 2005; Liu et al., 2015, 2016). It was believed that the basin has the coldest thermal regime in China and the basin is a typical "cold basin". The present-day geothermal gradient values range from 17.6 to 24 °C/km, with an average value of only 21.6 ± 2.9 °C/km at the depth interval of 0–5000 m. Based on the systematical temperature measurement and thermal conductivity of rocks data from documents (Wei, 1992; Wang et al., 1995a; Qiu, 2002; Wang L S, et al., 2005; Feng et al., 2009; Liu et al., 2015; Li et al., 2019, Li et al., 2020a, 2020b; Liu et al., 2020a, Liu et al., 2020b; Luo et al., 2020), 52 measured and calculated heat flow values were obtained in this study. The heat flow of the basin is between 27.4–66.5 mW/m^2 and the average value is 42.5 ± 7.6 mW/m^2 (Fig. 3a). Generally, the heat flow distribution relates well with basement undulation. The uplift area with shallow basement has higher heat flow (such as the southeastern basin, with heat flow over 60 mW/m^2). However, the heat flow value in the depression with thick sediments is relatively low with the values between 30–40 mW/m^2. There has some higher heat flow in the north part of basin (e.g., Kuqa Depression, >50 mW/m^2), and it is mainly resulted from thermal disturbance caused by reverse fault activity.

The heat flow distribution of the Sichuan basin is obtained based on the published 88 heat flow data (Wang et al., 1990; Han and Wu, 1993; Hu et al., 2000; Yuan et al., 2006; Xu et al., 2011; Jiang et al., 2016; Hu, 2020). The average heat flow of the basin is 53.8 ± 7.6 mW/m^2, and it is a "warm basin" (Fig. 3b). Generally, the heat flow value is high in the central and southeast parts of the basin and low in the north and northwest parts of the basin. The heat flow values are between 60–70 mW/m^2 in southwest and central basin, but it is 50–60 mW/m^2 in northwest basin and only 40–60 mW/m^2 in the north part of the basin.

There have been many studies of the present-day thermal gradient and heat flow of the Bohai Bay basin (Yang, 1985; Wang and Wang, 1988; Chen, 1988; Hu et al., 2000; Gong et al., 2003a, 2003b; Wang

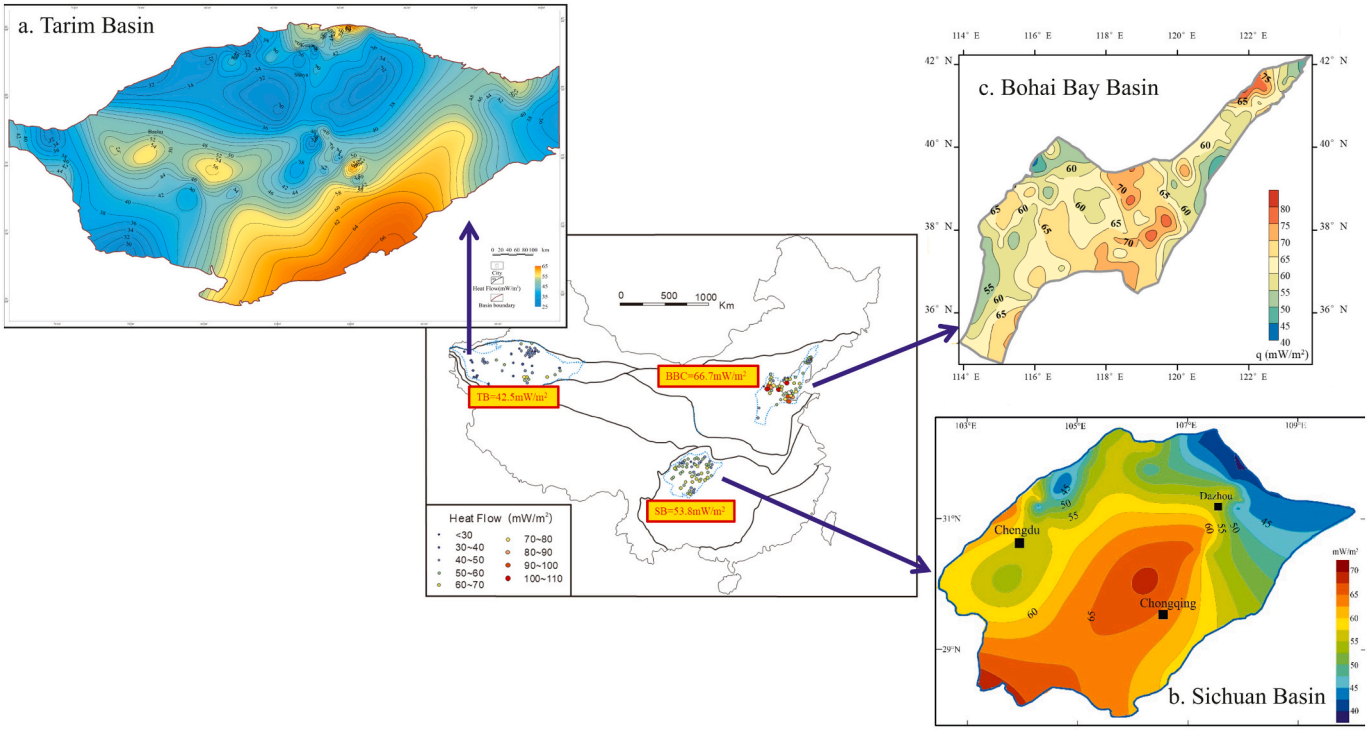

Fig. 3. Heat flow measurement points and heat flow distribution of the sedimentary basins in three Cratons of China.
a. Tarim Basin, b. Sichuan Basin, c. Bohai Bay Basin.

et al., 1985; Wang et al., 2002; Qiu et al., 2009, 2010; Zuo et al., 2011). The average present-day thermal gradient is 35 ± 4 °C/km for the entire basin. The heat flow of the basin is between 55–88 mW/m^2 based on 110 measured values and the average heat flow is 66.7 ± 8.1 mW/m^2. So, it is a typical "hot basin" (Fig. 3c). The Jiyang, Bozhong and Liaohe sub-basin of the eastern basin have relative high heat flow of 60–80 mW/m^2, and the heat flow value gradually decreases to the west of the basin. It decreases to 60–70 mW/m^2 in the Huanghua sub-basin and to 55–65 mW/m^2 in the Jizhong and Linqing sub-basins of the western basin.

3.2. Deep-temperature distribution at 10000 m

The distribution of deep temperature is very important for the analysis of source rock evolution, reservoir development and preservation of oil and gas phase. The temperature distribution over depth (geotherm) in the upper crust for the tectonically stable areas is primarily affected by conductive heat transport model (Chapman, 1986; Ehlers, 2005). The differential equation of time-dependent conductive heat transfer is:

$$-div(-K\nabla T)+A=\rho c\frac{\delta T}{\delta t} \tag{4}$$

where, T is temperature; t is time; K is thermal conductivity; A is volumetric heat production; ρ and c are density and specific heat, respectively. For one dimensional heat transfer in a homogeneous and isotropic medium with radiogenic heat production, Eq. (4) can be written as:

$$\frac{\delta^2 T}{\delta z^2}+\frac{A}{K}=\frac{1}{\alpha}\frac{\delta T}{\delta t} \tag{5}$$

where, α is the thermal diffusivity and defined by $\alpha = K/\rho c$. The most common simplification of the eq. (5) leads to the ordinary differential equation known as Poisson's equation:

$$\frac{d^2T}{\delta z^2}=-\frac{A}{K} \tag{6}$$

For the lithosphere, the heat production (A) varies with depth depending on the distribution of radioactive isotopes; and the thermal conductivity K is primarily determined by the composition although it is affected by temperature and pressure conditions (Ehlers, 2005; Chapman, 1986). For a layer with constant heat generation and thermal conductivity, the eq. (6) can be expressed as:

$$T(z)=T_0+\frac{q_0}{K}z-\frac{Az^2}{2K} \tag{7}$$

where, Z is the depth for temperature calculation (m); T_0 is the temperature at the basin's surface, taken as the annual average ground temperature of the basin; q_0 is the measured surface heat flow (mW/m^2); A is the heat production of rocks at the depth interval of 0 ~ Z (μW/m^3); and K is the thermal conductivity of rocks at the depth interval of 0 ~ Z (W/m·K).

At present, there are a number of exploration wells with a depth of over 8000 m and the presence of liquid hydrocarbons at this depth in Tarim Basin. We selected the 10,000 m depth to calculate deep temperature and obtained the distribution characteristics of temperature at this depth. The temperature at 10000 m depth were calculated using the formula (7) based on the burial depth, thermal conductivity and heat generation data of each stratum (Fig. 2) in three basins. The temperature at 10000 m depth in the Tarim basin distributes between 120 and 280 °C, and there is higher temperature at the north, southeast and

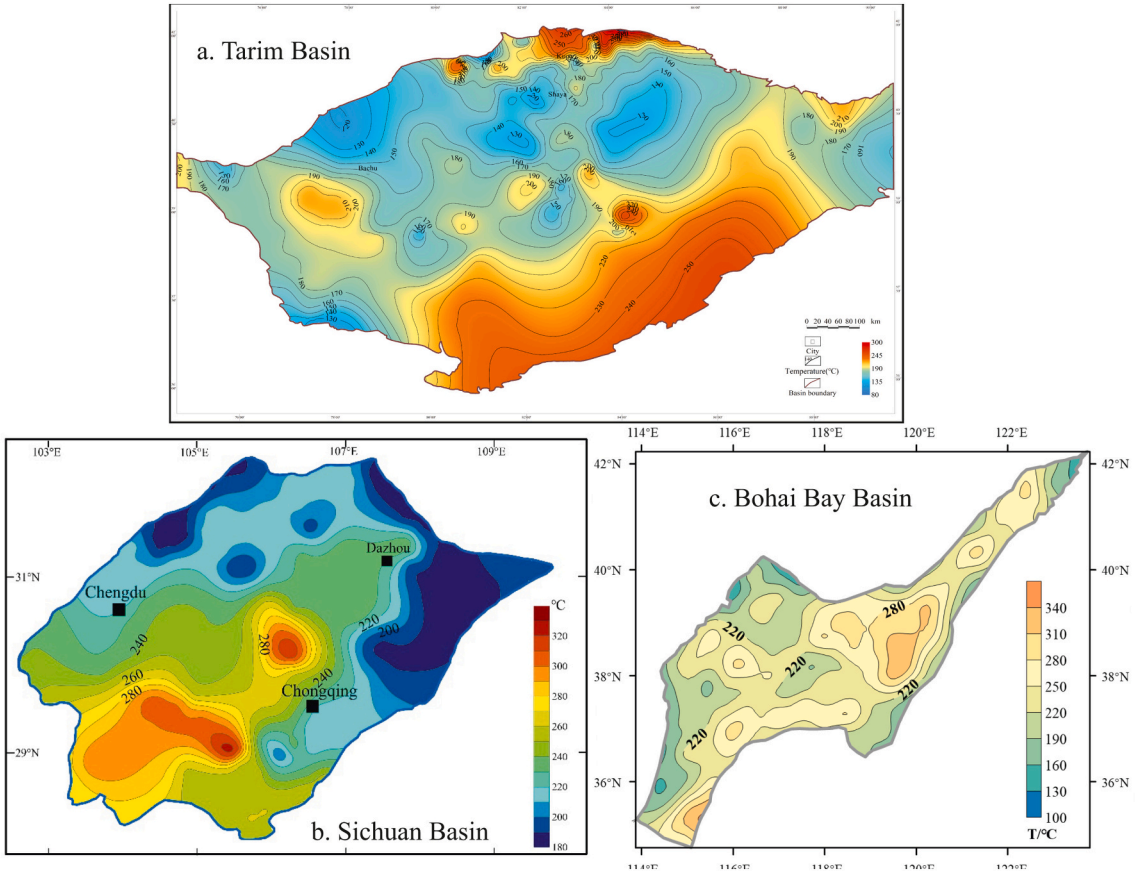

Fig. 4. Temperature distribution map at 10000 m depth.
a. Tarim Basin, b. Sichuan Basin, c. Bohai Bay Basin.

northwest parts of the basin (Fig. 4a). The temperature at 10000 m depth in the Sichuan basin distributes between 180 and 330 °C, and higher temperatures are located at the southwest and central parts of the basin, which is corresponding to the higher heat flow distribution (Fig. 4b). The temperature at 10000 m depth in the Bohai Bay basin distributes between 220 and 280 °C at most area, and the highest temperature of 340 °C are located at the Jiyang depression, east part of the basin (Fig. 4c).

3.3. Thermal structure of lithosphere and thermal lithospheric thickness

A thermal lithosphere is a type of lithosphere dominated by heat conduction (Morgan and Sass, 1984; Rudnick et al., 1998), and a thermal lithosphere's thickness is defined by the base of the thermal lithosphere as the intersection of a geotherm with the mantle adiabat Tm = 1300 °C (Rudnick et al., 1998; Artemieva and Mooney, 2001). The temperature of the thermal lithosphere varies with the depth and is also calculated by the one-dimensional thermal steady-state conduction eq. (7). The parameters to calculate thermal lithospheric thickness include geological parameters, thermo-physical parameters of the rocks, and thermal data. Thermal data usually include the surface temperature, surface heat flow, and heat flow history. The lithospheric thickness is between 76 and 102 km in the Bohai Bay Basin, eastern NCC (Qiu et al., 2016), and this thickness can be compared with those from the seismic observations of 70–90 km (Chen, 2009; Chen et al., 2009; Huang and Zhao, 2009; Tian et al., 2009). The lithospheric thickness of Sichuan Basin, Upper Yangtze Craton, is 130–140 km (Wang, 1996). However, Tarim Craton has the thickest lithosphere in the continental China with 140–170 km (Wang, 1996) (Table 1).

The thermal structure of the lithosphere is the ratio of crustal and mantle heat flow to surface heat flow or crustal to mantle heat flow (Blackwell, 1971). This ratio influences many energy-related processes, such as the activity of the crust and upper mantle, plate movement and deformation, and temperature at depth. The ratio of crustal or mantle heat flow to surface heat flow determines the type of the lithospheric thermal structure. According to the ratio of crustal to surface heat flow, Wang (1996) coined the terms "cold crust but hot mantle (CC-HM)" and "hot crust but cold mantle (HC-CM)" to describe the thermal structure of the lithosphere. When crustal heat flow accounts for over 50% of the surface heat flow in the study region, it is called the HC-CM structure. In this situation, the crust is thought to be relatively "hot" and the mantle is thought to be "cold". The opposite situation is called "cold crust but hot mantle".

We applied the "stripped-back" method provided by Wang and Wang (1988) to calculate the mantle heat flow in the regions of sedimentary basins based on the surface heat flow, the radioactive heat production rate and the thickness of crustal layers (Fig. 5a),

$$q_m = q_s - q_c = q_s - \sum A_i D_i \tag{8}$$

Here, q_c and q_m are the crustal and mantle heat flow (mW/m^2), respectively; q_s is the surface heat flow (mW/m^2); A_i is the radioactive heat production rate of the ith layer (μW/m^3); and D_i is the thickness of the ith layer (km). Fig. 5b gives an example of the calculation of the mantle heat flow. The mantle heat flow of 40.7 mW/m^2 was obtained by using formula (8), assuming a surface heat flow of 64 mW/m^2, a radioactive heat production rate and a thickness of each layer (Wang and Wang, 1988).

Table 1 shows the surface, crust and mantle heat flow of Tarim, Sichuan and Bohai Bay basins, respectively. According to the ratio of crustal to surface heat flow, Tarim Basin has a "hot crust but cold mantle (HC-CM)" type of the thermal structure of the lithosphere. The Sichuan Basin and Bohai Bay Basin are "cold crust but hot mantle (CC-HM)" type.

Table 1
Data of thermal statues in the basins in our study.

Basins	Tarim	Sichuan	North China
Surface Heat Flow (q_0, mW/m^2)	42.5	53.8	66.7
Heat Flow from curst (q_c, mW/m^2)	22.5	26.2	26.0
Heat Flow from mantle (q_m, mW/m^2)	20.0	27.6	40.7
q_m/q_0	47.0%	51.3%	61.0%
Type of thermal structure	HCCM	CCHM	CCHM
Thermal lithospheric thickness (km)	140–170	130–140	80–110

Notes: HCCM-hot curst and cold mantle; CCHM-cold curst and hot mantle.

4. Thermal history of sedimentary basins in cratons

4.1. Method and theory of the thermal history reconstruction

The thermal history of sedimentary basins can be reconstructed by the methods of thermal indicators (e.g., vitrinite reflectance and apatite fission track) and tectono- thermal evolution (e.g., stretching model of Mckenzie, 1978). The thermal indicators method is considered to be a more reliable method for thermal history reconstruction due to its constraints on the measured values of samples. Vitrinite reflectance (R_o) and fission track and (U—Th)/He data of apatite and zircon are widely used to establish the thermal evolution of sedimentary basins. However, there have no vitrinite macerals in the early Paleozoic strata and there is no apatite and zircon minerals in marine carbonate strata. In order to overcome these problems, some possible thermal indicators have been put forward, such as bitumen reflectance (R_b), vitrinite-like reflectance (R_v), graptolite reflectance (R_g), conodont alteration index (CAI), free radical density of organic matter, Laser Raman Spectroscopy of organic matter, thermoacoustic emission of rock. Now, equivalent vitrinite reflectance (R_{equ}), obtained by converting bitumen, vitrinite-like and graptolite reflectance, are widely used as the effective thermal indicators.

Apatite and zircon (U—Th)/He ages, AFT length and ages, and equivalent R_o data were used as thermal indicators in this study. The Easy%R_o model of R_o (Sweeney and Burnham, 1990) and the fan model of AFT annealing (Laslett et al., 1987) were applied. To model He ages, we applied the apatite model of Farley (2000) and the zircon model of Reiners et al. (2004). HeFTy software (version 2009) and Thermodel for Windows (version 2011), 1D for the forward and inverse models, were applied to model the thermal histories. The Thermodel software works with the AFT and R_o data of samples from multiple depths in a single well. By contrast, HeFTy software works with individual samples and integrates the AFT, (U—Th)/He and R_o data. The QtQt software can work with multiple samples and integrates the AFT, (U—Th)/He and R_o data in a single well. In our modeling, several thousand thermal paths were generated using the Monte Carlo inverse modeling method; the best-fit temperature path model identified the thermal history of the sample. A temperature path was regarded as the effective thermal history of a sample when the difference between the calculated and measured thermal indicator values was a minimum. The timing of tectonic thermal events and temperature paths, and possibly the burial history of the sample, could be constrained by the AFT data. Therefore, an average paleothermal gradient (G_t) from the top of the stratum to the sample depth could be calculated from the modeled paleotemperature (T_t) and the corresponding paleo-burial depth (Z_t) of the investigated samples (e.g., $G_t = (T_t\text{-}T_{surface})/Z_t$). The paleoburial depth of a sample could be obtained from the burial histories. This paleothermal gradient estimate is an average value over the depth interval from the paleoburial depth to the surface. Finally, the paleo-heat flow values are modeled based on the paleothermal gradient and the thermal conductivities of the individual strata.

4.2. Bohai Bay Basin in Eastern NCC

The Mesozoic thermal history is essential for understanding the lithospheric thinning and lithospheric thermal state in the eastern NCC. Because many oil companies explored the Paleogene and Neogene strata

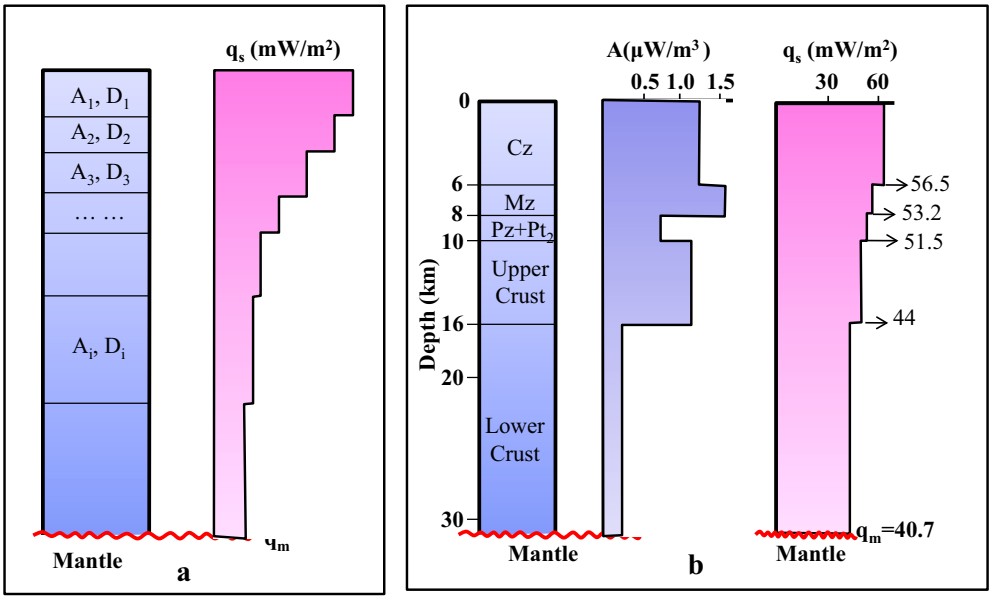

Fig. 5. a. Method of the mantle heat flow calculation. b. Mantle heat flow calculation result of the Bohai Bay basin (Wang and Wang,1988).

in the Bohai Bay Basin, previous studies of the thermal history of the basin have mainly focused on the Cenozoic thermal evolution (Hu et al., 1999, 2001; He and Wang, 2004; Qiu et al., 2004, 2006, 2007, 2010; Ding et al., 2008; Liu et al., 2018a; Liu and He, 2019), and the results have shown a cooling process in the Cenozoic. The Meso-Cenozoic thermal evolution of North China Craton (NCC) has also been studied (He, 2014, 2015; He and Zhang, 2018). Recent hydrocarbon exploration has begun to explore the deep Mesozoic and Paleozoic strata; however, there have been few studies of the Mesozoic thermal history of the basin (Li and Liao, 2001; Fu et al., 2004; Yao et al., 2006; Hu et al., 2007; Qiu et al., 2014, 2016).

As a thermal history reconstruction sample, Well Y155, located in the Jiyang sub-basin, is shown to reconstruct Meso-Cenozoic heat flow evolution by using thermal indicators of R_o data (Fig. 6). The results of the thermal history reconstruction show that it had a lower heat flow value (52 ± 5.2 mW/m^2) during the Early Mesozoic (Fig. 6e). The heat flow gradually increased, reaching a peak value of 85 ± 8.8 mW/m^2 during the late Early Cretaceous, and then it gradually decreased to 68 ± 6.8 mW/m^2 during the Late Cretaceous. Due to the extensional rift phase in the Paleogene, the heat flow increased again. The well experienced a second heat flow peak value of 88 ± 7.8 mW/m^{2}during the Middle and Late Paleogene. The heat flow decreased again after the basin entered a thermal subsidence phase during the Neogene.

With the thermal history reconstruction of different wells, the Meso-Cenozoic thermal evolution of the basin was obtained (Fig. 7). The basin experienced a lower and stable heat flow of 53 ± 5.3–58 ± 5.8 mW/m^2 during the Triassic and Jurassic, which is consistent with the heat flow of the Proterozoic craton (55 ± 17 mW/m^2 from Rudnick et al., 1998). The heat flow increased drastically after the beginning of the Cretaceous and experienced the first heat flow peak in the end of the Early Cretaceous with a surface heat flow of 82 ± 8.2–86 ± 8.6 mW/m^2, which is consistent with evidence from the tectonic evolution, magmatic petrology and geochemistry (Wu et al., 2005b; Zhai et al., 2005; Zhu et al., 2008). The basin experienced the post-rift thermal decay period in the Late Cretaceous, which began to decrease gradually to 65 ± 6.5 to74 ± 7.4 mW/m^2 in the Late Cretaceous. The basin again entered an extensional rift phase in the Paleocene, and heat flow increased again during this period (Qi et al., 1995; Qi and Yang, 2010; Allen et al., 1997). It reached its second heat flow peak during the Eocene and Oligocene with a heat flow of 81 ± 8.1 to 88 ± 8.8 mW/m^2. Finally, the basin experienced the post-rift thermal decay in the Neogene and Quaternary accompanied by a gradual decrease of the surface heat flow to the present-day values of 57 ± 5.7 to 65 ± 65 mW/m^2. Magmatic activity decreased drastically, and the heat flow decreased with the extinction of the rift structure prior to the Neogene. However, because the thick Neogene and Quaternary sediments have an insulating effect, the basin retains the previously higher heat flow.

4.3. Sichuan Basin in UYC

Studies on the thermal regime of the Sichuan Basin have been conducted since the 1980s (Xie and Yu, 1988; Huang and Wang, 1991; Han and Wu, 1993; Xu et al., 2011). In recent years, with the number of boreholes increasing, many deep stratum temperature data were collected, which provided the study basis on geothermal regime in the region. Recently, many studies have been carried out in the thermal history reconstruction of the Sichuan basin (Qiu et al., 2008; Zhu et al., 2010, 2015, 2016, 2018, 2019; He et al., 2011; He et al., 2014; Huang et al., 2012; Xu et al., 2018; Liu et al., 2018a, 2018b; Jiang et al., 2018; Hu, 2020), and thermal evolution since the Sinian was obtained.

Fig. 8 shows a single well's thermal history modeling result. For the well MX13, the simulation results of R_o matched well with the measured data suggesting the high credibility of modeling process (Fig. 8). It experienced a lower and stable heat flow of 56 mW/m^2 during the Sinian to the early Permian period. The heat flow reached to the maximum at the end of Early Permian exceeded 80 mW/m^2 and then it decreased to 63 mW/m^2 at present-day.

There are differences in heat flow evolution among different tectonic units in Sichuan Basin. But they all experienced the stable heat flow stage before the Early Permian, the rapid rising stage of heat flow in the end of the Early Permian, heat flow decline stage after the Late Permian (Fig. 9). The heat flow at the Early Paleozoic was about 50–55 mW/m^2 in the Western depression, and there was a heat flow peak at the end of Early Permian, with the heat flow of 80–115 mW/m^2, which resulted from the activity of Emeishan Plume (He et al., 2014; Zhu et al., 2015, 2016, 2018). After that, the heat flow decreased rapidly. The heat flow at the Early Paleozoic was about 55–60 mW/m^2 in the Central basin, and there was a heat flow peak at the end of Early Permian, with the heat flow of 82–95 mW/m^2. There are lower heat flow evolutions in the Northern and Eastern Basin with the feat flow peak values of 62–75 mW/m^2 at the end of Early Permian. However, the overall heat flow evolution of the southern Sichuan is relatively stable. The heat flow

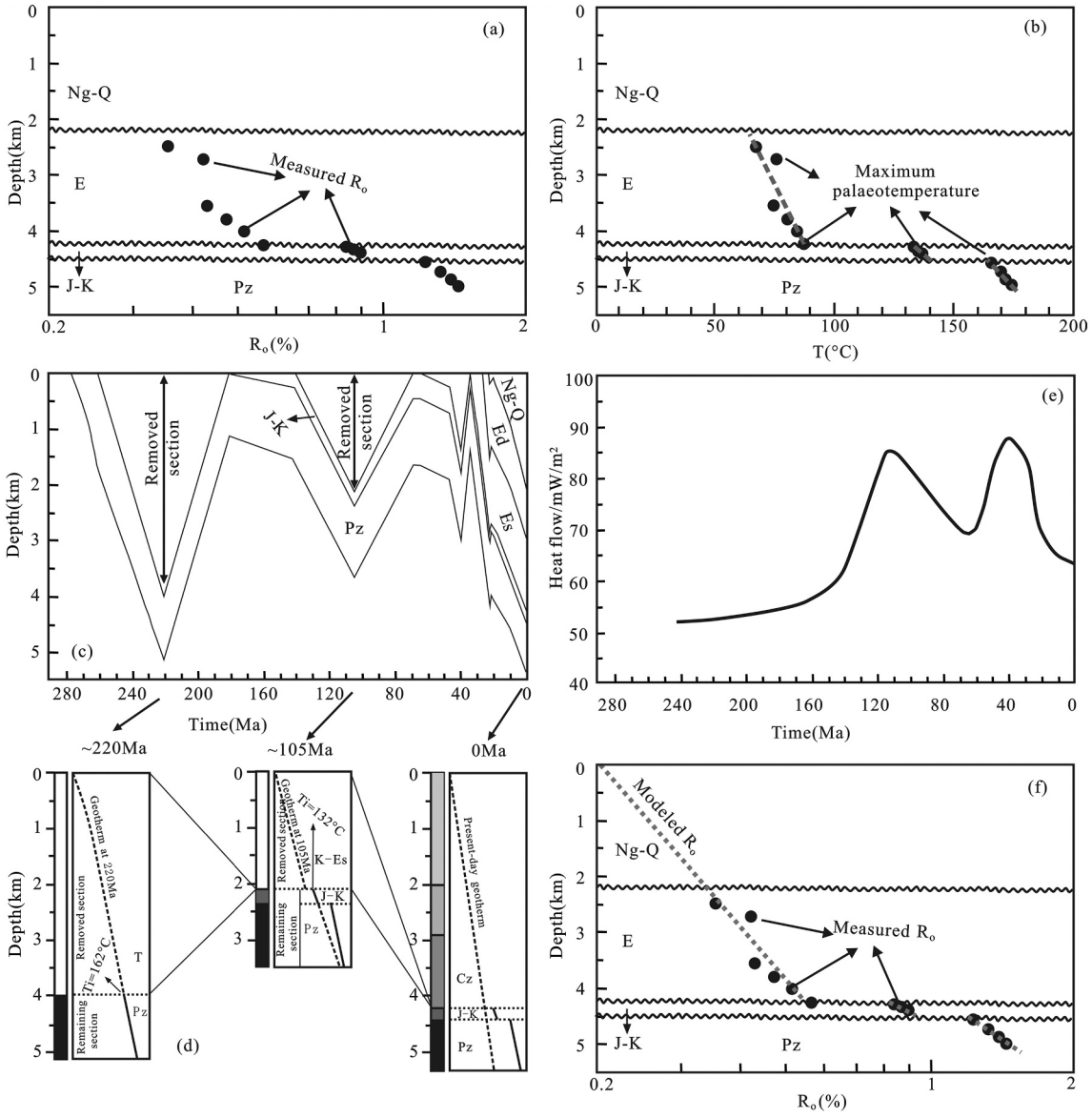

Fig. 6. The modeled results of the thermal history of well Y155 in the Bohai Bay Basin (From Qiu et al., 2016).
a. Vitrinite reflectance profile, b. Calculated maximum paleo-temperatures based on the Ro values and Easy%Ro method, c. Burial history, d. Paleo-temperature profiles for typical time, e. Reconstructed thermal history, and f. The best fit of the measured and predicated vitrinite reflectance.

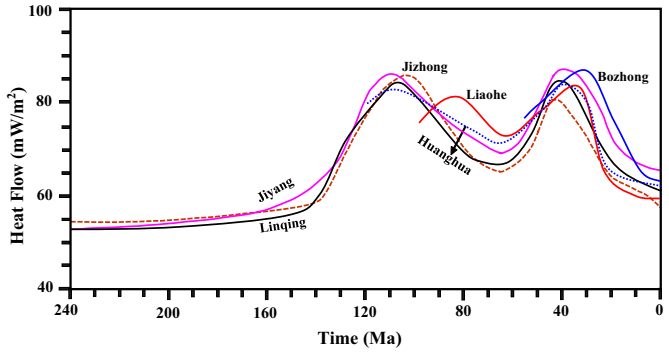

Fig. 7. Meso-Cenozoic thermal history of several sub-basins in the Bohai Bay Basin (From Qiu et al., 2016).

slightly increased in the middle and Late Permian, and then decreased to 50–60 mW/m^2 at present-day.

Affected by the thermal effect of Emeishan mantle plume (or Large igneous province, LIP), there was a heat flow peak in the Permian in Sichuan Basin. However, the peak value of heat flow is related to the distance from the center of mantle plume. Southwest Sichuan, near the center of mantle plume, has obviously high abnormal heat flow value, but the peak value of heat flow in northeast Sichuan, far from the mantle plume, is relatively low or has no effect (Qiu et al., 2008; Zhu et al., 2010, 2015, 2016, 2018, 2019; He et al., 2011, He et al., 2014; Huang et al., 2012; Xu et al., 2018; Liu et al., 2018a, 2018b; Jiang et al., 2018; Hu, 2020).

4.4. Tarim Basin in TC

Some previous thermal history studies have indicated a cooling trend to the thermal history of the basin with a thermal gradient decreasing from ~40 °C/km or high heat flow values during the Early Paleozoic to 20–25 °C/km in the present-day (Pan et al., 1996; Xie and Zhou, 2002; Li

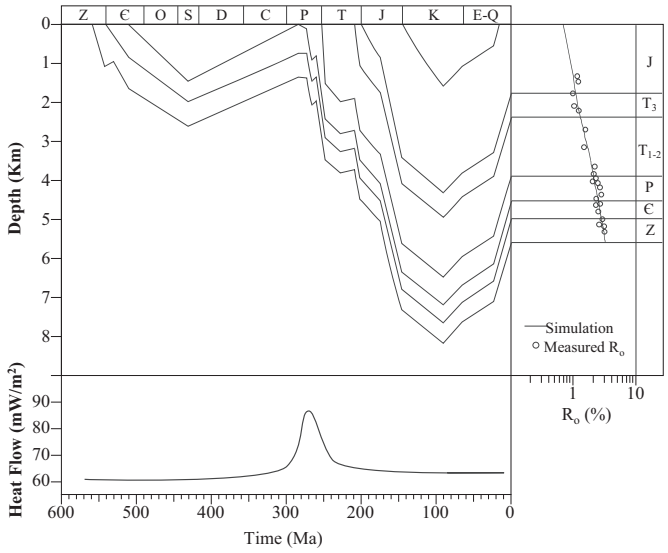

Fig. 8. Burial and thermal history for well MX13 in the Sichuan Basin (Liu W, et al., 2018).

et al., 2004, 2005, 2010; Xiao et al., 2008; Chang et al., 2014, 2016, 2017, 2019), whereas other studies have indicated a cold basin with thermal gradients of approximately 20 °C/km during the Early Paleozoic, which is almost the same as present-day conditions (Tu, 1994; Jin, 1997). The following will introduce the thermal paths of single sample, multi-samples and single well's thermal history.

4.4.1. *Sample KQ1-1 (2402.1 m, S_{2y})*

The thermal history of the sample was modeled using helium ages and AFT data. The apatite helium ages and AFT data all suggested extensive tectonic uplift during the Cretaceous. Two thousand thermal paths were tried with the Monte Carlo inverse modeling method and a best-fit temperature-time path was obtained (Fig. 10). Combining the modeled temperature with the burial depth of the sample during the Silurian, a Silurian thermal gradient of 34–37 °C/km was calculated. The sample reached 95–105 °C at the end of the Devonian, and the depth of the sample was approximately 2400 m at that time based on the burial history. The average thermal gradient was approximately 31–35 °C/km in the Devonian. The sample reached a maximum temperature of 130–140 °C at a burial depth of 3700 m in the Late Carboniferous with the paleothermal gradient being 30–32 °C/km at that time. A gradient of 27–28 °C/km at the end of the Cretaceous decreased to the present-day gradient of 20 °C/km.

4.4.2. *Well HT1*

Thermal paths were modeled using the QtQt software and AFT data from several samples in Well HT1 of Central Tarim Basin (Fig. 11). The thermal history shows that there experienced a rapid cooling event during the Late Cretaceous to Early Eocene (75-50 Ma) with cooling rate of ~8 °C/Ma. And it was followed by a rapid sedimentary process at the

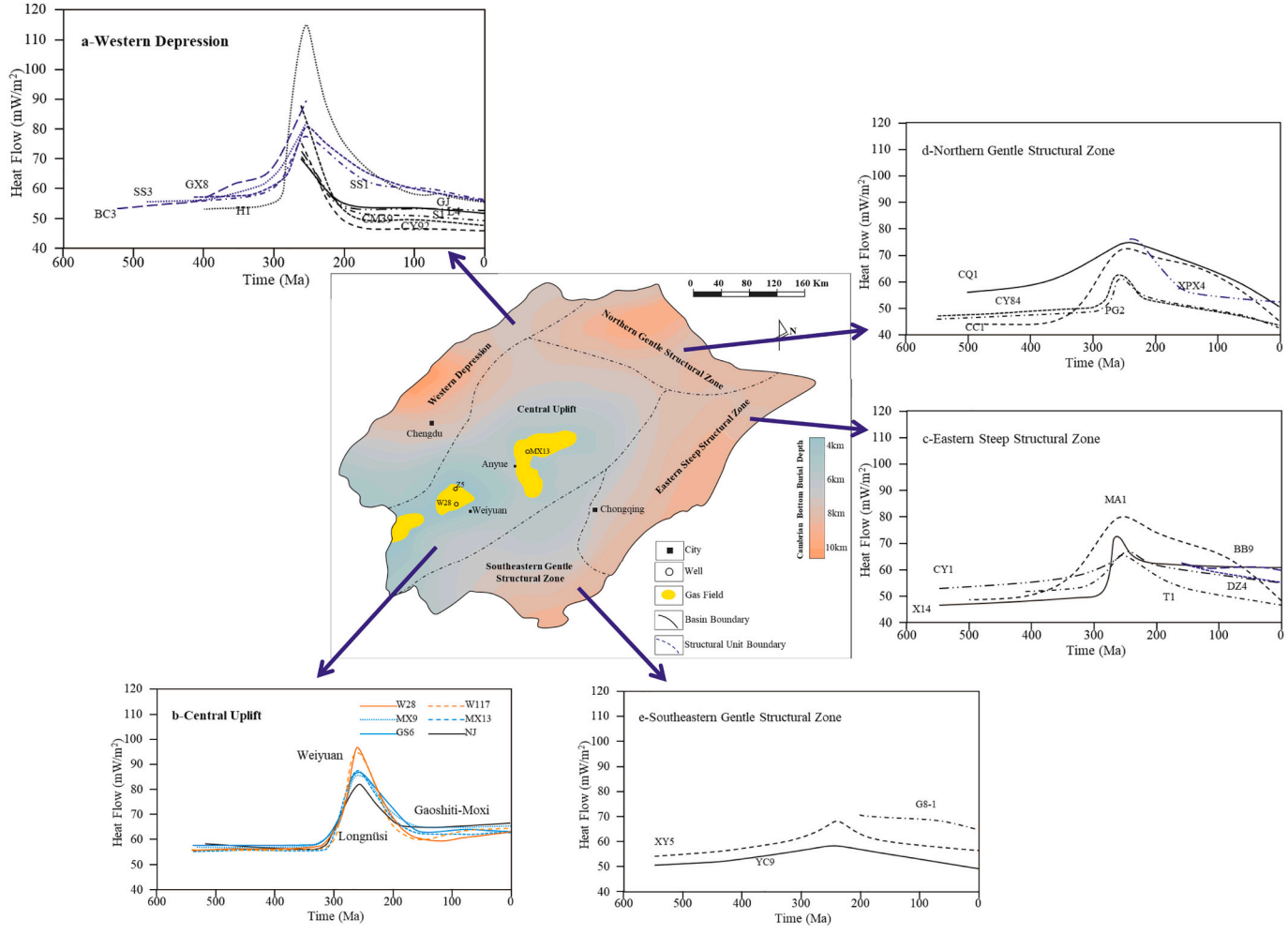

Fig. 9. Thermal histories of different tectonic units of Sichuan Basin.

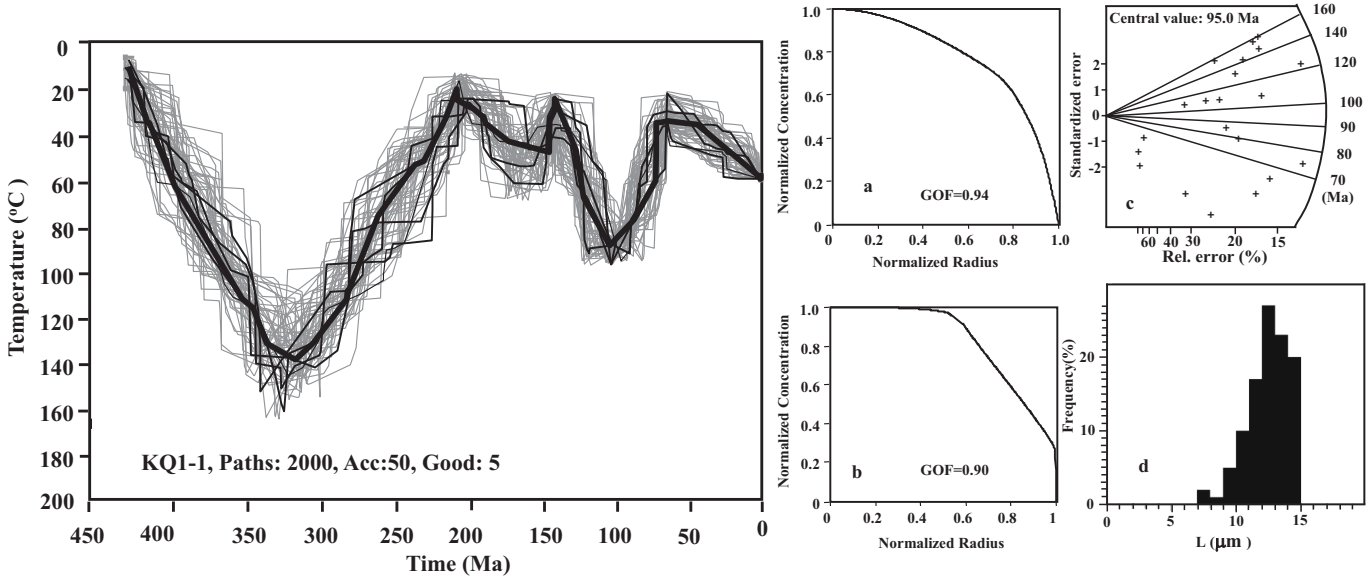

Fig. 10. Thermal history of sample Kq1-1(2402.1 m, S) in KQ1 well in the Tarim Basin (From Qiu et al., 2012).
2000 thermal paths were tried using the Monte Carlo inverse modeling method, and 50 paths are accepted (gray lines) and 5 paths are good (thin black lines). The thick black line is the "best" temperature path. GOF = Goodness of fit.
a. Apatite helium diffusional profile, b. Zircon helium diffusional profile, c. Apatite fission track ages and d. Apatite fission track length distribution.

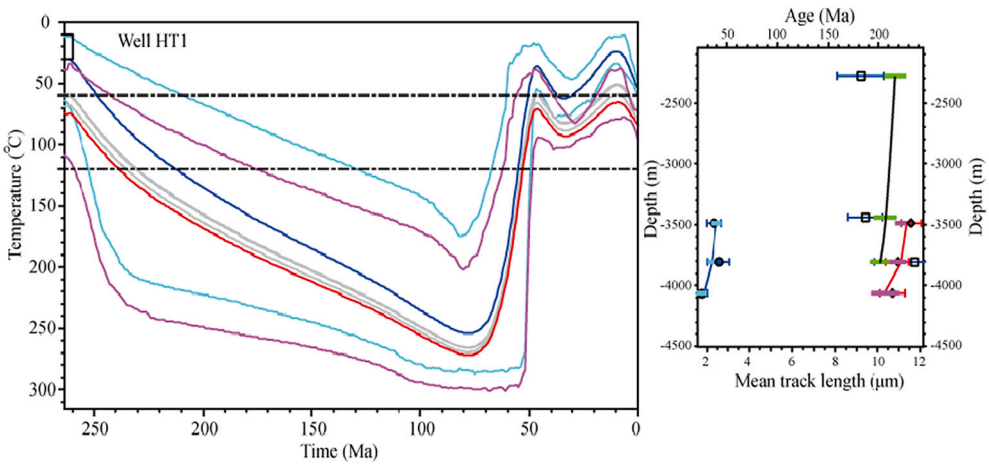

Fig. 11. Thermal history of Well HT1 in the Bachu Uplift of Tarim Basin by QtQt software.
The blue, gray and red lines represent the uppermost, middle and lowermost samples in the thermal paths. Two light blue lines represent the 95% confidence interval of the thermal history path of the uppermost sample. Two magenta lines represent the 95% confidence interval of the thermal history path of the lowest sample. (For interpretation of the references to colour in this figure legend, the reader is referred to the web version of this article.)

period of 50–35 Ma, and the temperatures of samples increased to 70–100 °C. After that, there experienced a slow uplift and denudation event from Oligocene to Miocene (30-10 Ma).

4.4.3. *Well TZ1*

The well TZ1 is located in the Central Uplift of the basin. The thermal history was modeled using the Thermodel software based on R_{equ} data. The TZ1 well has an unconformity between the Upper Ordovician and Carboniferous units. It also shows a clear offset between the Lower Ordovician and the Carboniferous in the R_{equ}-depth profile. The slope of R_{equ}-depth curve in the Cambrian-Lower Ordovician strata is greater than that of strata above the unconformity, indicating a higher thermal gradient during the Early Paleozoic than the Late Paleozoic and Mesozoic (Fig. 12). When the thermal indicator values (R_{equ}, AFT) corresponded well with the measured values, the supposed thermal history path was regarded as being correct, and the thermal history of a well could be simulated. The modeled R_{equ} fit well with the measured values in TZ1 well (Fig. 12). The modeled results of well TZ1 shows that the Cambrian and Ordovician units experienced their highest temperatures in the Late Ordovician and then decreased gradually after the Caledonian event. The thermal gradients also decreased gradually to the present-day gradients.

There has been a decreasing heat flow during the entire geological history, but the thermal history evolved differently in the different structural zones. There were higher heat flow values in the eastern and central basin (e.g., wells TD1, T1, H4 and TZ1) than in the north part of the basin (e.g., wells S47, LN5 and ST1) during the Early Paleozoic (Fig. 13). The Tarim Basin developed initially as a cratonic peripheral aulacogen resulting from the opening of the paleo-Asian Ocean in the Cambrian and the Early Ordovician. The stretching and thinning of the crust resulted in high heat flow at that time. In our study, the heat flow of the Cambrian and Early Ordovician in the eastern and central basin is 60–70 mW/m^2. The cratonic periphery aulacogen disappeared when the paleo-Asian ocean was closed in the Late Ordovician. Subsequently, the basin entered an interior cratonic phase in the Silurian, and the heat flow decreased gradually from the Silurian to the Permian. However, there experienced a heat flow peak at the end of Early Permian in some structural units (e.g., well T903), which may be caused by the thermal

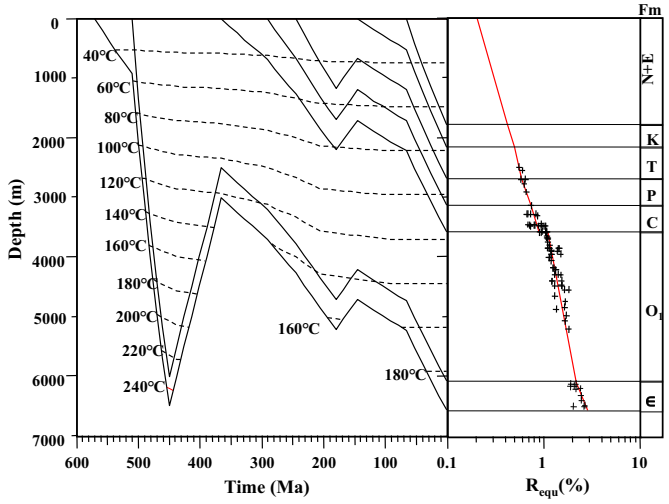

Fig. 12. The burial and thermal history of Well TZ1 in the Tarim Basin. The measured (+) and modeled R_{equ} values (black line) in right figure.

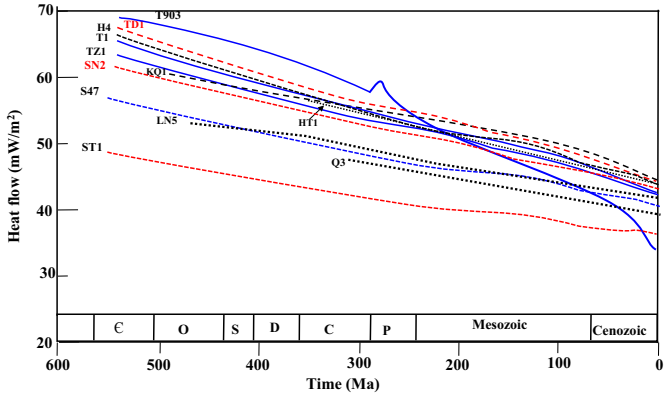

Fig. 13. Thermal gradient evolution in the studied wells of the Tarim basin. Some previous study results are also listed, T903 and S47—Li et al. (2010), LN5-Pan et al. (1996) and Q3-Wang et al.(2003).

effect of Permian LIP as in Sichuan Basin (Li et al., 2016). Since the Triassic, the basin experienced the formation of a foreland basin during the Mesozoic and Cenozoic periods, and the heat flow decreased continuously to its present-day value of 42 mW/m^2.

5. Discussion

In this section, we will focus on the thermal characteristics of typical cratons around the world, including the comparation of heat flow, lithospheric thermal structure and thermal lithospheric thickness. Since Siberian craton is a typical stable craton and Wyoming craton is a typical destructed craton in the world, we take them as representatives of stable cratons and broken cratons, and compare them with ENCC, including heat flow and thermal lithospheric thickness evolution. In addition, thermal evolution of Cambrian source rocks in the Tarim and Sichuan Basins also discussed in this section.

5.1. Thermal regime comparation between stable and destabilized cratons

Cratons are widely distributed in the world (Fig. 14). Most cratons are stable because of its low density, low water content and thick lithospheric root. The rigidity of the lithosphere ensures that it remains stable during the later reformation. However, some cratons were destroyed during Phanerozoic and lost the stable feature of the craton (e.g., NCC and Wyoming Craton). Generally, the process of losing the stability of a craton is called destruction (Wu et al., 2008), or decratonization or destabilization (Yang et al., 2009). Heat is closely related to the activity of the craton, and the following will discuss the different thermal regimes between the stable and destroyed cratons.

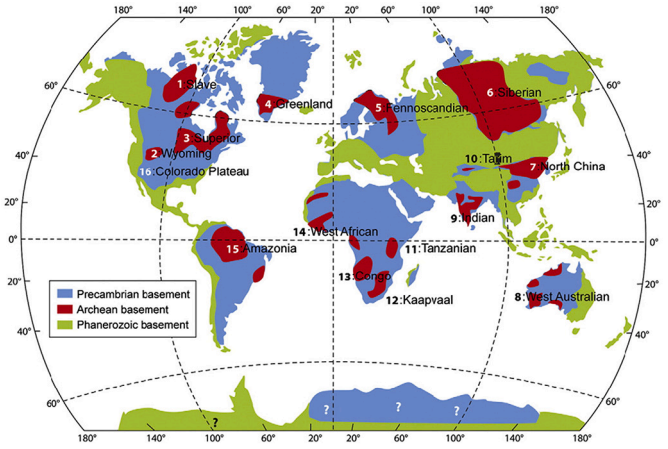

Fig. 14. Distributions of global Archean cratons (After Tang et al., 2013; Kusky and Polat, 1999).

5.1.1. Present-day's heat flow of typical cratons

Using data from the Global Heat Flow Database provided by the University of North Dakota (http://www.heatflow.und.edu/), heat flow in the typical Archean cratons was analyzed. Most cratons exhibit low heat flow values in the range of 35 to 50 mW/m^2, including the Tarim Craton of China, India Dharwar Craton, Western Gawler, Pilbara and Yilgarn Cratons of Australia, Slave and Superior Cratons of North America, Amazon Craton of South America, and the African, European and Siberian Cratons. However, some cratons exhibit higher heat flow values in the range of 59 to 65 mW/m^2 than that of certain typical cratons from around the world, such as the eastern NCC and the Wyoming Craton (Fig. 15). High heat flow values are generally the result of cratonic destruction, lithospheric thinning and radiogenic heat production in the crust. The eastern NCC and Wyoming Craton both underwent destruction in the Mesozoic-Cenozoic. The destruction was accompanied by lithospheric thinning, which leads to high heat flow values.

5.1.2. Heat flow evolution of typical stable and destructed cratons

Besides thermal indicators, thermobarometer can be used to study the mineral inclusions and xenoliths within the lithosphere to provide an estimation of the paleo-heat flow. The temperature estimated from the mantle xenoliths is consistent with that of surface heat flow estimation, based on the study of the Archean Craton (Rudnick et al., 1998; Mackenzie and Canil, 1999). The heat flow values from the mantle xenoliths shows a stable heat flow of 40 ± 5 mW/m^2 in the stable cratons (Fig. 16), which is basically consistent with the current heat flow data. However, the destroyed cratons have also the lower and stable heat flow values at the early stage of evolution, but they have higher values of heat flow after the craton is broken. The thermal history of craton relied on above thermal history reconstruction and the mantle xenoliths heat flow in this study. Here, we selected the eastern NCC and Wyoming Craton to represent the destructive craton category, and the Siberian Craton to represent the stable cratons (Fig. 17).

5.1.2.1. The eastern NCC. The eastern NCC experienced some complicated thermal history. It had a lower and stable heat flow during the Paleozoic, based on the evidence from litho-geochemistry data (Menzies et al., 1993; Griffin et al., 1998; Zheng et al., 2005). Mantle xenoliths and diamond inclusions revealed that heat flow was only 36–40 mW/m^2

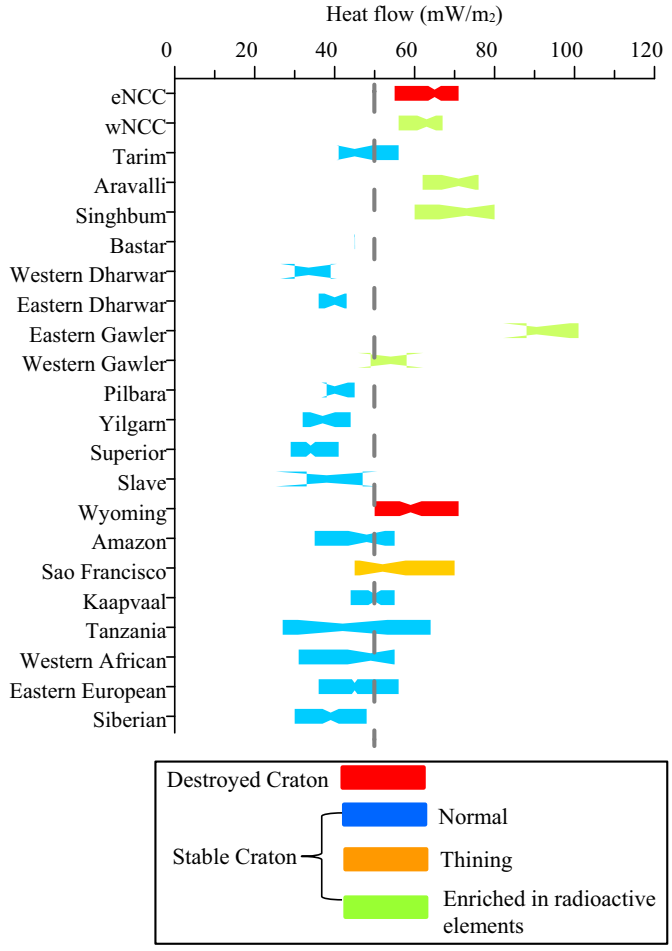

Fig. 15. The heat flow distribution of cratons in global (From Xu and Qiu, 2016).

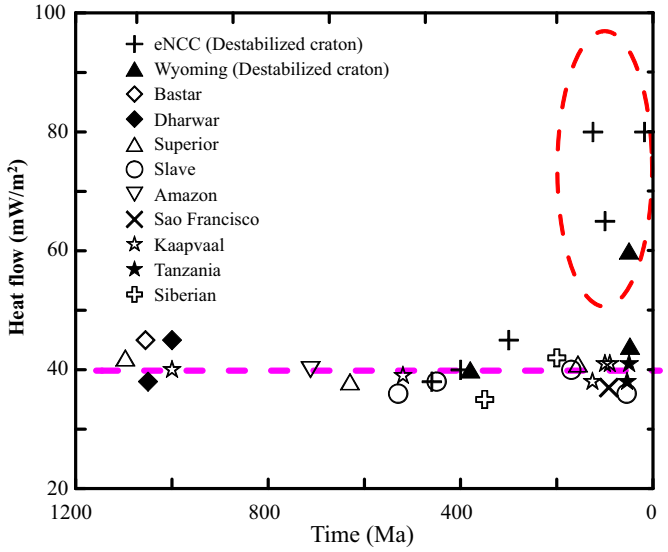

Fig. 16. The ratio of crustal to mantle heat flow with different cratons.

at Paleozoic (440–490 Ma) (Griffin et al., 1998), and then the heat flow increased gradually during the Triassic and Jurassic. The thermal history reconstructed by the thermal indicators method in the previous section revealed that heat flow experienced two heat flow peaks in the end of the Early Cretaceous and during the Eocene and Oligocene, with a surface heat flow of 81–88 mW/m^2, and a heat flow peak of 80 mW/m^2 (at 120 Ma) is corresponding to the value from mantle xenoliths (Zheng et al., 2005, 2007). Most importantly, the history of heat flow can be used to date the timing of loss of the lithospheric root on the eastern NCC. This will be discussed in the following section.

5.1.2.2. The Wyoming Craton. The Wyoming Craton, located in the northwest of the USA, is composed predominantly of Late Archean rocks (3.2–3.5Ga) and appears to have undergone cratonization during extensive magmatism from 2.5–2.9 Ga (Foster et al., 2006). The craton has undergone progressive destruction after the subduction of the Farallon plate and remained unstable since the Meso-Cenozoic. A heat flow value of approximately 40 mW/m^2 at 380 Ma was calculated from the Sloan xenoliths (Eggler et al., 1987). The craton had a low heat flow value until the end of Mesozoic, and then heat flow increased dramatically. Peridotite xenoliths from the Eocene Homestead kimberlite pipe (~50 Ma) indicated a much hotter Eocene geotherm approaching 60 mW/m^2 (Irving et al., 2003), and the heat flow value has been maintained until now.

5.1.2.3. The Siberian Craton. The Siberian Craton is formed by an assemblage of Archean and Proterozoic basement. Final stabilization of the Siberian Craton took place approximately 1.9–1.8 Ga after large-scale volcanic activity occurred, and then a series of intra-cratonic sedimentary basins were formed. Heat flow within the Siberian Craton exhibited some changes in the Phanerozoic, however, the magnitude of these changes was relatively small. It experienced a stable heat flow during the Paleozoic. According to an analysis of xenoliths from Late Paleozoic kimberlite fields (360–344 Ma) and Mesozoic kimberlite fields (245–135 Ma), heat flow during these time periods can be estimated approximately 35 mW/m^2 and 40–45 mW/m^2, respectively (Taylor et al., 2003; Rosen et al., 2009). The heat flow increase is due to the magmatism caused by the mantle plume activity during the period of early Mesozoic (245–240 Ma). Since the Late Mesozoic, the heat flow has been continuously reduced to about 25 mW/m^2, while the Anabar shield has the lowest heat flow values ranging from 15 to 25 mW/m^2 (Duchkov, 1991).

5.1.3. Thermal structure of lithosphere of typical stable and destructed cratons

Usually, the destroyed cratons have higher mantle heat flow values (>25 mW/m^2), but the stable cratons have lower mantle heat flow values (<25 mW/m^2). We calculated the ratio of crustal to mantle heat flow (q_c/q_m) for different cratons. Fig. 18 illustrates that q_c/q_m is greater than 1.0 for most stable cratons (Tarim, Dharwar, Gawler, Pilbara, Superior, Kaapvaal, and Siberian cratons), but less than 1.0 in the destroyed cratons (Wyoming Craton and NCC). The Gawler craton have abnormal high q_c/q_m value, which may result from high concentration of heat generating elements in crust (Neumann et al., 2000). The lithosphere's thermal structure reflects the activity strength of different cratons. The eastern NCC and Wyoming Craton possess a CC-HM structure, which shows that these regions have relatively strong activity. Other cratons including the Tarim, Superior, Kaapvaal, Eastern Europe and Siberian Cratons, have an HC-CM structure that corresponds with relative stability in the cratonic lithosphere.

5.1.4. Thermal lithospheric thickness evolution of typical stable and destructed cratons

Thermal lithospheric thickness can be calculated from mantle xenoliths and the method of heat conduction. Lithospheric thicknesses of cratons calculated from mantle xenoliths show that the lithosphere of most stable cratons has been stable since Archean (>180 km) (Fig. 19). And from the global cratonic thermal lithosphere thickness, ENCC and WC have thin thermal lithosphere thickness (<150 km), but the thermal

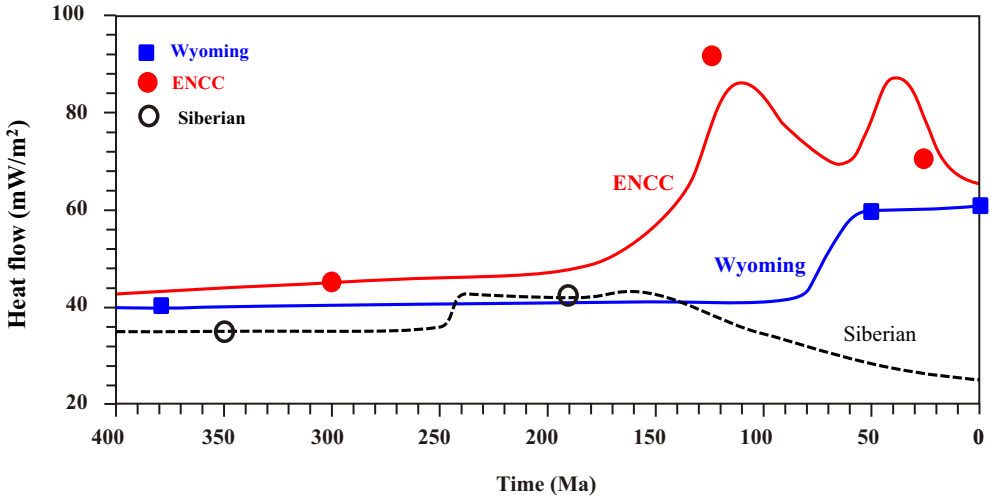

Fig. 17. Paleo-heat flow values of cratons calculated from mantle xenoliths.
The dashed line is average heat flow of 40 mW/m^2, and the broken circle is the region of high heat flow.

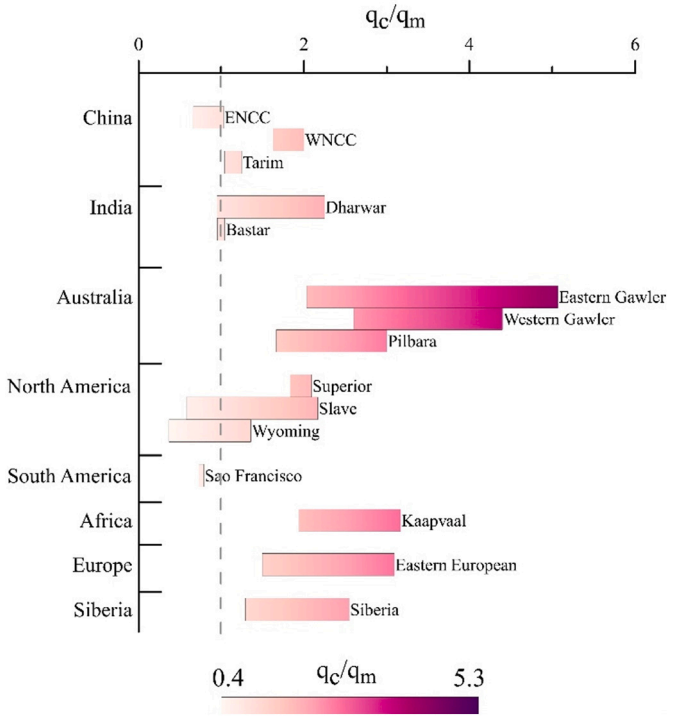

Fig. 18. Heat flow evolution of different cratons.
The solid circle, solid square and circle are heat-flow values calculated from mantle xenoliths in the ENCC, Wyoming and Siberian cratons. The Meso-Cenozoic heat flow of ENCC was reconstructed by Ro and AFT data (Qiu et 2014,2015). The Paleozoic and Cenozoic heat flow data are from references (Irving et al., 2003; Eggler et al., 1987).

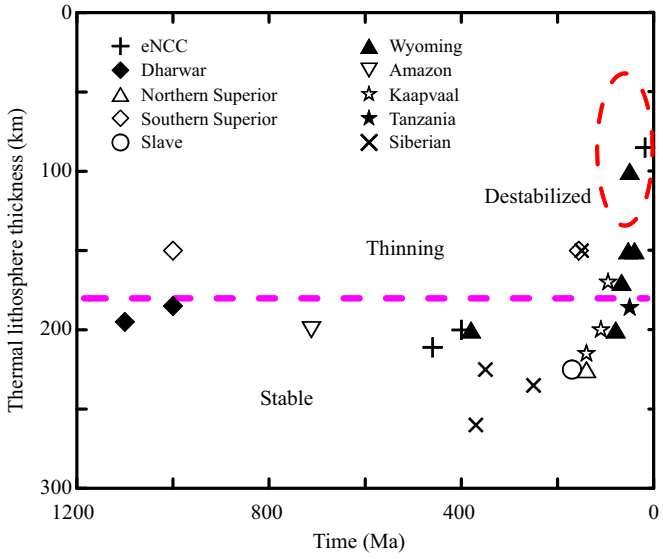

Fig. 19. Lithospheric thicknesses of cratons calculated from mantle xenoliths.

lithosphere thickness of most other cratons is mainly 150–300 km (Fig. 20). Based on the above thermal histories and paleo-heat flow values from mantle xenoliths, the thermal lithospheric thickness evolutions were calculated in the eastern NCC, Wyoming and Siberian Cratons as followings.

The ENCC had a thick lithosphere of approximately 200 km in the Paleozoic. Thereafter, the lithosphere began to thin and reached a thinning peak (~51 km) in the late Early Cretaceous. The thickness then increased to approximately 80 km at the end of the Cretaceous. With the development of a rift phase in the Bohai Bay basin, the lithosphere experienced a second thinning peak in the Middle and Late Paleogene (~48 km). The lithosphere thickened thereafter and is currently 78 km or so (Fig. 21). This lithospheric thinning since Mesozoic has been confirmed by geophysics and petrochemistry evidences (Menzies et al., 1993; Griffin et al., 1998; Huang et al., 2009; Tian et al., 2009).

In the Paleozoic, the thermal thickness of the lithosphere remained steady at approximately 250 km at the Owl Creek uplift of the Wyoming Craton. This situation changed in the Late Mesozoic when the Farallon plate began its eastward subduction. During the early Eocene (~50 Ma) the lithosphere's thermal thickness decreased to approximately 105 km and remained stable since the Late Eocene (Fig. 21). This evolution is consistent with data from xenoliths and other researches (Eggler et al., 1987; Carlson et al., 1999; Irving et al., 2003; Artemieva, 2006). The lithosphere's thickness calculated from the Sloan xenoliths was approximately 200 km at 380 Ma (Eggler et al., 1987). Mantle xenoliths from the Eocene Homestead kimberlite (~50 Ma) estimates the lithospheric mantle's root falling between 85 and 120 km (Irving et al., 2003). Extensive igneous activity inboard from the western edge of North America during 54–45 Ma suggested that injection of the

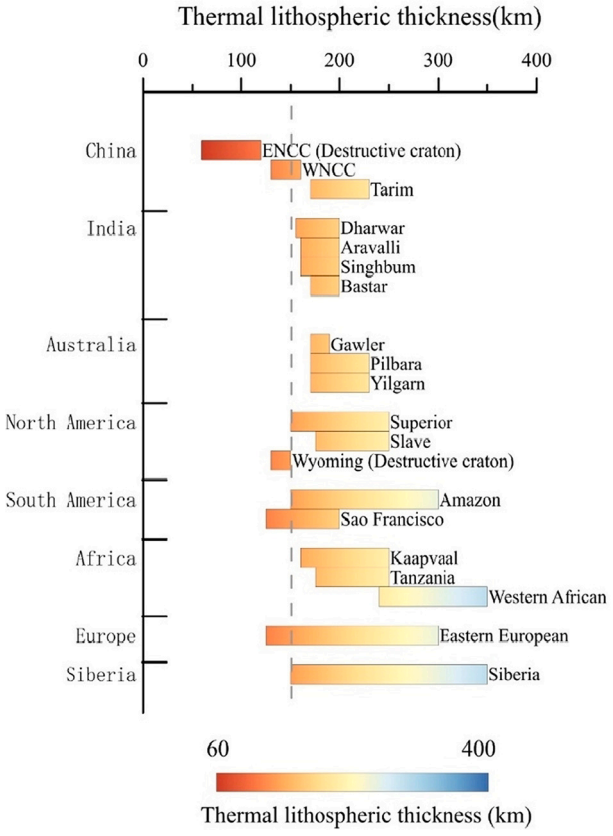

Fig. 20. The thermal lithosphere thickness distribution of cratons in global.

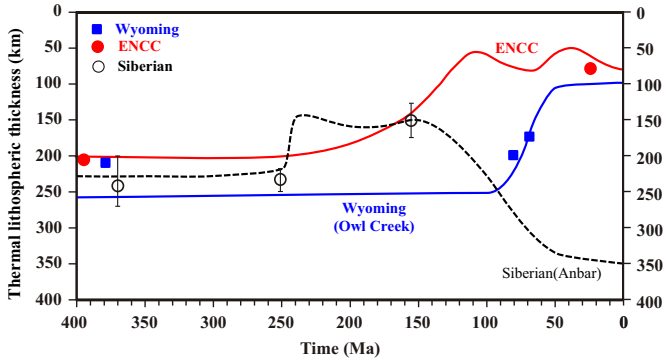

Fig. 21. The evolution of lithospheric thicknesses of typical cratons.

asthenosphere was accompanied either by thermal erosion or delamination of the lithospheric root of the Wyoming Craton (Dudas and Harlan, 1999).

The thermal thickness of the lithosphere at the Anabar Shield of the Siberian Craton experienced the thinning process during the Mesozoic (Fig. 21). The mantle xenoliths in kimberlites revealed a thick lithosphere (200–220 km) in Paleozoic (360 Ma). During the early Mesozoic (245–240 Ma), the thermal thickness decreased to approximately 150 km as a result of kimberlite magmatism, and the kimberlite xenoliths from 160 Ma revealed a lithospheric thickness of about 150 km (Taylor et al., 2003). Since the late Jurassic, the lithosphere's thermal thickness has gradually increased, and it is currently 350 km.

In general, heat flow is closely related to the thickness of thermal lithosphere. The heat flow value is higher in the area with small thickness of thermal lithosphere. At the same time, heat flow can be used to date the timing of loss of the lithospheric root or lithosphere thinning. These two heat flow peaks in the end of the Early Cretaceous and during the Eocene and Oligocene correspond to two thinning peaks of the lithosphere in the NCC. Therefore, heat flow provides theoretical geothermal evidence for craton destruction.

5.2. *Thermal evolution of Cambrian marine source rocks in the Tarim and Sichuan Basins*

The Cambrian is one of the most important hydrocarbon source rocks in the Tarim and Sichuan Basins. Based on the heat flow, burial depth and one-dimensional steady-state heat conduction equation, the temperature at the bottom of Cambrian is calculated in these basins. The temperature at the bottom of Cambrian of Tarim basin distribute between 80 and 260 °C, and the area with temperature lower 160 °C are mainly located in the north and northwest parts of the basin. However, the temperature at the bottom of Cambrian can be up to 260 °C at the east part of the basin due to the deep burial and high heat flow values in these areas (Fig. 22a). The bottom of Cambrian of Sichuan basin is at temperature of 120–180 °C in most areas (Fig. 22b). At the same time, the Cambrian experienced different heating evolution between Tarim and Sichuan basins. The Cambrian in the Tarim Basin experienced rapid heating during the Cambrian and Ordovician period (heating rate of 1 °C/Ma) and slow continuous heating (heating rate of 0.1 °C/Ma) from Silurian to present (Fig. 23a). However, The Cambrian in Sichuan Basin experienced a complicated heating evolution, rapid heating during the Cambrian and Ordovician period (0.9 °C/Ma), heating stagnation during the Silurian and Carboniferous, rapid heating again during the Permian and Early Cretaceous period (0.9 °C/Ma), and finally continuous cooling stage from the Late Cretaceous to present (Fig. 23b).

Hydrocarbon generation history was established using burial profiles and thermal histories from the two basins in the study. Burial history was modeled using BasinMod software provided by Platte River Associates, Inc. (PRA), and the Easy%R_o maturity model. The basic premise of the Easy%R_o model is that R_o is related to the chemical composition of kerogen (Sweeney and Burnham, 1990). However, the thermal effect of Permian LIP should be considered when simulating the mature evolution of Cambrian source rocks in this study. There is no influence from the Permian LIP in the Tarim Basin. However, the influence of source rock evolution from the Permian LIP in Sichuan Basin depends on the distance from Emeishan mantle plume (Fig. 24). Wells MS1 and JS1 are far from mantle plume, and the maturity evolution of Cambrian source rocks is not affected by Permian LIP; But wells HS1 and YF1 are near the mantle plume, the maturity evolution of Cambrian source rocks is affected by Permian LIP, and its maturity increased rapidly in the Late Permian (Fig. 24).

The Cambrian in the Tarim basin entered maturity threshold (R_o = 0.5%) at the beginning of the Ordovician. It entered the middle maturity stage at the Middle Ordovician (R_o = 0.7%) and late mature at the Late Silurian. Finally, the source rock entered the main gas generation stage (R_o = 1.3%) at the Middle Carboniferous (Fig. 25a). The Cambrian in the Sichuan basin entered maturity threshold (R_o = 0.5%) at the beginning of the Ordovician. It entered the middle maturity stage at the Middle Silurian (Ro = 0.7%) and late mature at the Late Permian (R_o = 1.0%). Finally, the source rock entered the main gas generation stage (R_o = 1.3%) at the Early Jurassic (Fig. 25b).

In generally, thermal history is the key parameter to determine the mature evolution and hydrocarbon generation of source rocks and cold basin and hot basin show different evolution paths of source rock maturity. The thermal regime and thermal history of the main cratonic basins in this paper can provide a basis for the evolution of deep to ultra-deep and Cambrian source rock series, and at the same time, may also provide a basis for the study of ultra-deep oil and gas phase state. Although the contribution of Permian LIP thermal effect to the evolution of source rocks in Tarim and Sichuan basins is different, the overall impact on the time and space of source rocks evolution is limited. The lowest temperature at 10000 m depth in Tarim Basin, a typical cold

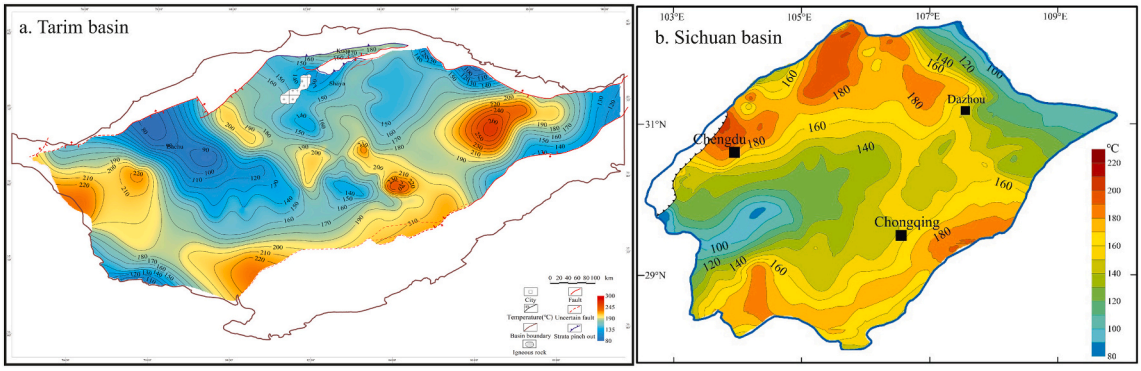

Fig. 22. Present-day's temperature distribution at the bottom of the Cambrian.
a. Tarim basin, b. Sichuan basin.

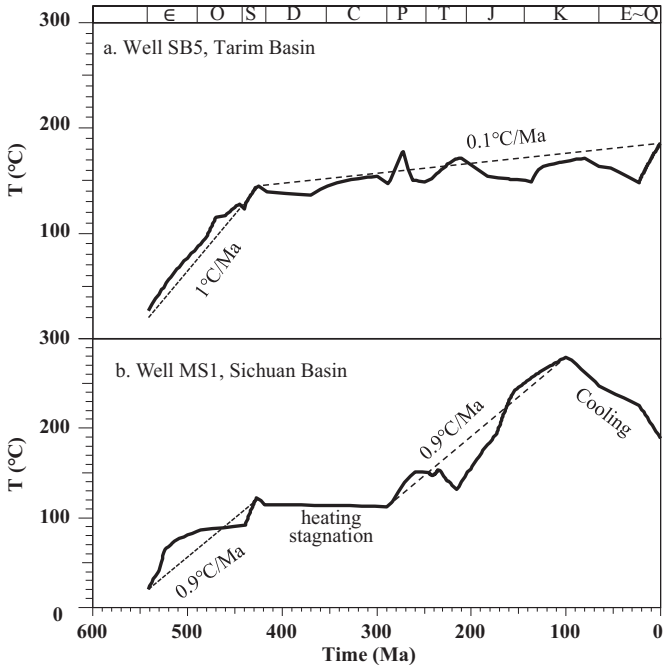

Fig. 23. Thermal evolution and heating rate at the bottom of the Cambrian for typical wells in the Tarim basin (a) and Sichuan basin (b).

basin, is only 120–140 °C, which is still in the temperature range of liquid window. In other words, there can still be temperature conditions for the wide distribution of liquid hydrocarbons in the ultra-deep layer of Tarim Basin. This is of great significance to guide oil exploration. Therefore, the review of thermal regime and thermal history in this paper provides an important decision-making basis for deep and ultra-deep oil and gas exploration.

5.3. *Problems in thermal history reconstruction*

At present, there are still a series of problems in the reconstruction of

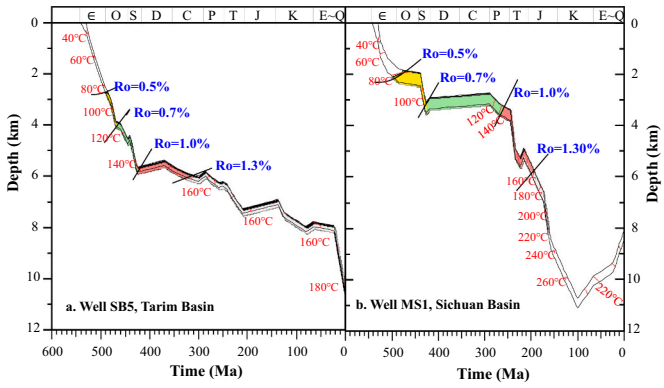

Fig. 25. The thermal evolution of the Cambrian source rocks in the Tarim and Sichuan Basins.

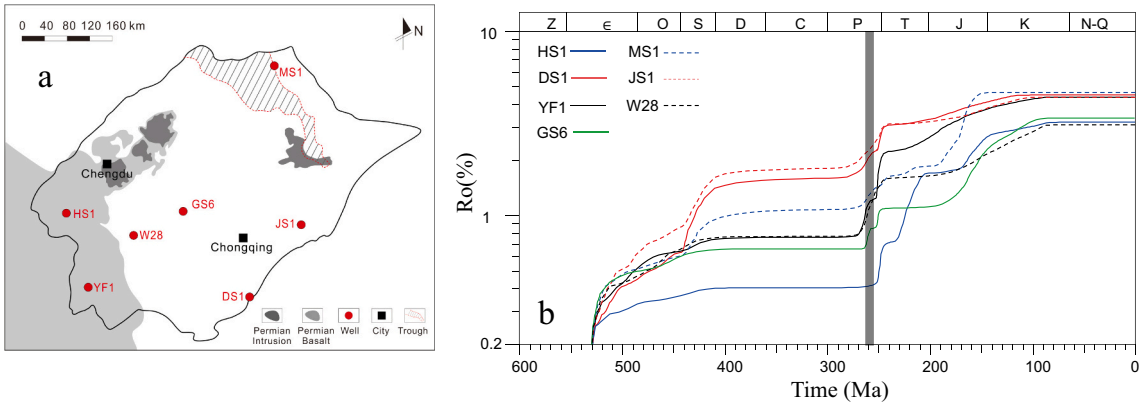

Fig. 24. The thermal evolution of the Cambrian source rock in the typical wells in the Sichuan Basins. a. Locations of typical wells and the distribution of Permian igneous, b. Maturity evolution of seven typical wells.

thermal history of deep, ultra-deep, marine strata and Pre-Late Paleozoic strata. Effective thermal indicator, which the recorded thermal information can be retained to present-day, is the core issue of thermal history reconstruction. However, the early thermal information recorded by the ultra-deep thermal indicators is mostly reset by the late deep burial and high temperature. Especially, the older the stratigraphic age, the harder it is to save the early thermal information. Even if the early thermal information can be saved, there are many influencing factors in the inversion of thermal history, and the thermal history uncertainty obtained from the simulation also increases. At present, low temperature thermochronology is considered to be an effective method to solve the complex thermal history. But the key is to obtain apatite and zircon mineral from marine strata. Clastic strata are developed in Sinian and Lower Paleozoic marine strata in the Sichuan basin, and apatite and zircon mineral samples can be obtained for low temperature thermochronology analysis. In addition, the cluster isotope is the most promising method to study the thermal history of marine carbonate strata (Xu et al., 2019; Liu et al., 2020a, 2020b).

6. Conclusions

(1) The heat flow and thermal status in three typical cratons in the continental of China are 42.5 ± 7.6 mW/m^2 in the Tarim Craton (cold basin), 53.8 ± 7.6 mW/m^2 in the Upper Yangtze Craton (warm basin) and 66.7 ± 8.1 mW/m^2 in the eastern NCC (hot basin), respectively.
(2) The temperature at 10000 m depth were distributes between 120 and 280 °C in the Tarim basin, 180–330 °C in the Sichuan basin and 220–280 °C in the Bohai Bay basin.
(3) The lithospheric thickness is between 76 and 102 km in the Bohai Bay Basin, eastern NCC, 130–140 km in the Sichuan Basin and 140–170 km in the Tarim Basin. The Tarim Basin has a HC-CM type, but the Sichuan Basin and Bohai Bay Basin are CC-HM type of the thermal structure of the lithosphere.
(4) Thermal histories show that the Bohai Bay basin experienced a lower and stable heat flow of 53 ± 5.3–58 ± 5.8 mW/m^2 during the Triassic and Jurassic, and then developed two heat flow peaks in the end of the Early Cretaceous and at the Eocene and Oligocene with heat flow of 81–88 mW/m^2; The Sichuan Basin experienced the stable heat flow stage before the Early Permian, the rapid rising stage of heat flow in the end of the Early Permian, heat flow decline stage after the Late Permian. However, the Tarim Basin has been a decreasing heat flow during the entire geological history, but the thermal history evolved differently in the different structural zones.
(5) Most stable cratons in the world exhibit low heat flow values in the range of 35 to 50 mW/m^2, some destroyed cratons exhibit high heat flow values in the range of 59 to 65 mW/m^2. Usually, the destroyed cratons have higher mantle heat flow values (>25 mW/m^2) with CC-HM structure, but the stable cratons have lower mantle heat flow values (<25 mW/m^2) with HC-CM structure.
(6) Heat flow evolution obtained by the thermal indicators, mineral inclusions and xenoliths show that the eastern NCC experienced a lower and stable heat flow during the Paleozoic, and two heat flow peaks in the end of the Early Cretaceous and during the Eocene and Oligocene, with a surface heat flow of 81–88 mW/m^2; The Wyoming Craton had a low heat flow value until the end of Mesozoic, and then heat flow increased dramatically and maintained until now. The Siberian Craton experienced a stable heat flow during the Paleozoic, and increased to 40–45 mW/m^2 in Mesozoic and then continuously reduced to about 25 mW/m^2, Since the Late Mesozoic.
(7) Thermal lithospheric thickness of destructed cratons experienced a thinning process from approximately 200 km to 78 km in the eastern NCC, from approximately 250 km to 100 km in the Wyoming Craton, but the stable Siberian Craton experienced a lithospheric thickening process from 150 km at Mesozoic to 350 km currently.
(8) Different thermal histories and heating rates controlled the maturation evolution of Cambrian marine source rocks in the Tarim and Sichuan Basins. There can still be temperature conditions for the wide distribution of liquid hydrocarbons in the ultra-deep layer of Tarim Basin.

Declaration of Competing Interest

The authors declare that they have no known competing financial interests or personal relationships that could have appeared to influence the work reported in this paper.

Acknowledgement

The National Natural Science Foundation of China (Grant No. U19B6003, 41830424) and National Key Research & Development Program of China (Grant no. 2017YFC0603102)

References

Ali, J.R., Fitton, J.G., Herzberg, C., 2010. Emeishan large igneous province (SW China) and the mantle-plume up-doming hypothesis. J. Geol. Soc. 167, 953–959.
Allen, M.B., MacDonald, D.I.M., Zhao, X., Vincent, S.J., Menzies, C.B., 1997. Early Cenozoic two-phase extension and late Cenozoic thermal subsidence and inversion of the Bohai Basin, North China. Mar. Pet. Geol. 14, 951–972.
Artemieva, I.M., 2006. Global 1°×1° thermal model TC1 for the continental lithosphere: implications for lithosphere secular evolution. Tectonophysics 416 (1), 245–277.
Artemieva, I.A., Mooney, W.D., 2001. Thermal thickness and evolution of Precambrian lithosphere: a global study. J. Geophys. Res. 106, 16387–16414.
Blackwell, D.D., 1971. The thermal structure of the continental crust. In: Heaoock, J.G. (Ed.), The Structure and Physical Properties of the Earth Crust. AGU, Washington, D. C, pp. 169–184.
Carlson, R.W., Irving, A.J., Hearn, J.R.B.C., 1999. Chemical and isotopic systematics of peridotite xenoliths from the Williams kimberlite, Montana: clues to processes of lithosphere formation, modification and destruction. In: Proceedings of the 7th International Kimberlite Conference, Cape Town: Red Roof Design, pp. 90–98.
Chang, J., Roderick, B., Yuan, W.M., Li, W.Z., Que, Y.Q., Qiu, N.S., 2014. Mesozoic cooling history of the "Bachu Uplift" in the Tarim Basin, China: constraints from zircon fission-track thermochronology. Radiat. Meas. 67, 5–14.
Chang, J., Li, J.W., Qiu, N.S., Song, X.Y., Li, H.L., 2016. Multiple cooling episodes in the Central Tarim (Northwest China) revealed by apatite fission track analysis and vitrinite reflectance data. International Journal of Earth Science 105 (4), 1257–1272.
Chang, J., Tian, T., Qiu, N.S., 2017. Mid-late Miocene deformation of the northern Kuqa fold-and-thrust belt (southern Chinese Tian Shan): An apatite (U-Th-Sm)/He study. Tectonophysics 694, 101–113.
Chang, J., Li, D., Kyle, M., Qiu, N.S., Xiao, Y., Wu, H., Liu, N., 2019. Cenozoic deformation of the Kalpin fold-and-thrust belt, southern Chinese Tian Shan: new insights from low-T thermochronology and sandbox modeling. Tectonophysics 766, 416–432.
Chapman, D.S., 1986. Thermal gradients in the continental crust. Geol. Soc. Lond., Spec. Publ. 24 (1), 63–70.
Chapman, D.S., Pollack, H.N., 1975. Global heat flow: a new look, Earth Planet. Sci. Lett. 28, 23–32.
Chen, M.X., 1988. Geothermics of Northern China (in Chinese with English Abstract). Science Press, Beijing.
Chen, L., 2009. Lithospheric structure variations between the eastern and central North China Craton from S- and P-receiver function migration. Phys. Earth Planet. Inter. 173, 216–227.
Chen, L., Cheng, C., Wei, Z.G., 2009. Seismic evidence for significant lateral variations in lithospheric thickness beneath the central and western North China Craton. Earth Planet Science Letters 286, 171–183.
Cheng, C., Chen, L., Yao, H.J., Jiang, M.M., Wang, B.Y., 2013. Distinct variations of crustal shear wave velocity structure and radial anisotropy beneath the North China Craton and tectonic implications. Gondwana Res. 23, 25–38.
Ding, Z.Y., Wang, L.S., Hu, W.X., Zhang, P., Liu, S.W., Mi, N., 2008. Reconstruction of Cenozoic thermal history of Bohai Bay basin with a transient heat flow model. Acta Pet. Sin. 29, 650–656 (in Chinese with English abstract).
Duchkov, A.D., 1991. Review of Siberian Heat Flow Data. Springer, Berlin, pp. 426–443.
Dudas, F.Ö., Harlan, S.S., 1999. An Ancient Depleted Mantle Sample from a 42 Ma Dike in Montana: Constraints on Persistence of the Lithosphere during Eocene Magmatism. The Journal of Geology 107, 287–299.
Eggler, D.H., Mccallum, M.E., Kirkley, M.B., 1987. Kimberlite-transported nodules from Colorado-Wyoming; a record of enrichment of shallow portions of an infertile lithosphere. Geol. Soc. Am. Spec. Pap. 215, 77–90.
Ehlers, T.A., 2005. Crustal thermal Processes and the Interpretation of Thermochronometer Data. Rev. Mineral. Geochem. 58 (1), 315–350.

Farley, K.A., 2000. Helium diffusion from apatite: General behavior as illustrated by Durango fluorapatite. J. Geophys. Res. 105, 2909–2914.
Feng, C.G., Liu, S.W., Wang, L.S., Li, C., 2009. Present day geothermal regime in Tarim basin, Northwest China. Chin. J. Geophys. 52 (11), 2752–2762.
Foster, D.A., Mueller, P.A., Mogk, D.W., et al., 2006. Proterozoic evolution of the western margin of the Wyoming craton: implications for the tectonic and magmatic evolution of the northern Rocky Mountains. Can. J. Earth Sci. 43 (10), 1601–1619.
Fu, M.X., Hu, S.B., Wang, J.Y., 2004. Thermal regime transition in eastern North China and its tectonic implication. Science in China (D) 34, 514–520 (in Chinese).
Furlong, K., Chapman, D.S., 1987. Thermal state of the lithosphere. Rev. Geophys. 25, 1255–1264.
Gong, Y.L., 2003. The Thermal Structure and Thermal Evolution of Bohai Bay Basin in East China, Ph.D. Dissertation. Nanjing University, Nanjing, China (in Chinese).
Gong, Y.L., Wang, L.S., Liu, S.W., Li, C., Han, Y.B., Li, H., Liu, B., Cai, J.G., 2003a. Distribution characteristics of heat flow in Jiyang depression, Shandong, North China. Sci. Sin. Terrae 33, 383–391 (in Chinese).
Gong, Y.L., Wang, L.S., Liu, S.W., Guo, L.Z., Cai, J.G., 2003b. Distribution characteristics of Geotemperature field in Jiyang depression, Shandong, North China. Chinese J. Geophysics 46, 652–658 (in Chinese with English abstract).
Griffin, W.L., Andi, Z., O'Reilly, S.Y., et al., 1998. Phanerozoic Evolution of the Lithosphere Beneath the Sino-Korean Craton. Washington, D.C. Am. Geophy. Union 107–126.
Guo, X.S., Hu, D.F., Huang, R.C., Wei, Z.H., Duan, J.B., Wei, X.F., Fan, X.J., Miao, Z.W., 2020. Deep and ultra-deep natural gas exploration in the Sichuan Basin: Progress and prospect. Nat. Gas Ind. 40 (5), 1–14.
Han, Y.H., Wu, C.S., 1993. Geothermal gradient and heat flow values of some deep Wells in Sichuan basin. Oil Gas Geol. 14 (1), 80–84 (in Chinese with English abstract).
Han, Q.S., Peng, S.B., Kusky, T., Polat, A., Jiang, X.F., Cen, Y., Liu, S.F., Deng, H.A., 2017. Paleoproterozoic ophiolitic melange, Yangtze craton, South China: evidence for Paleoproterozoic suturing and microcontinent amalgamation. Precambrian Res. 293, 13–38.
He, L.J., 2014. Numerical modeling of convective erosion and peridotite-melt interaction in big mantle wedge: Implications for the destruction of the North China Craton. Journal of Geophysical Research-Solid Earth 119 (4), 3662–3677.
He, L.J., 2015. Thermal regime of the North China Craton: Implications for craton destruction. Earth Sci. Rev. 140, 14–26.
He, L.J., Wang, J.Y., 2004. Tectono-thermal modelling of sedimentary basins with episodic extension and inversion, a case history of the Jiyang Basin, North China. Basin Res. 16, 587–599.
He, L.J., Zhang, L.Y., 2018. Thermal evolution of cratons in China. J. Asian Earth Sci. 164, 237–247.
He, D.F., Jia, C.Z., Li, D.S., Zhang, C.J., Meng, Q.R., Shi, X., 2005. Formation and evolution of polycyclic superimposed Tarim basin (in Chinese): Oil and Gas. Geology 25, 64–76.
He, L.J., Xu, H., Wang, J.Y., 2011. Thermal evolution and dynamic mechanism of the Sichuan Basin during the early Permian-Middle Triassic. Sci. China: Earth Sci. 54, 1948–1954.
He, L.J., Huang, F., Liu, Q.Y., Li, C.R., Wang, J.Y., 2014. Tectono-thermal evolution of Sichuan basin in early Paleozoic. J. Earth Sci. Environ. 36 (2), 10–17.
Hou, G.T., Qian, X.L., Cai, D.S., 2001. The tectonic evolution of Bohai basin in Mesozoic and Cenozoic time. Acta Sci. Nat. Univ. Pekin. 37, 845–851 (in Chinese with English abstract).
Hu, D., 2020. Thermal Regime and Maturity Evolution of the early Paleozoic Source Rocks in the Southwest Sichuan Basin, Southwest China. Dissertation of the University of Chinese Academy of Sciences 22–37.
Hu, S.B., Zhang, R.Y., Luo, Y.H., 1999. Thermal history and tectono-thermal evolution of the Bohai Basin. Chin. J. Geophys. 42 (6), 748–755.
Hu, S.B., He, L.J., Wang, J.Y., 2000. Heat flow in the continental area of China: a new data set. Earth Planet. Sci. Lett. 179, 407–419.
Hu, S.B., Paul, B.O.S., Asaf, R., Barry, P.K., 2001. Thermal history and tectonic subsidence of the Bohai Basin, northern China: a Cenozoic rifted and local pull–apart basin. Phys. Earth Planet. Inter. 126, 221–235.
Hu, S.B., Fu, M.X., Yang, S.C., Yuan, Y.S., Wang, J.Y., 2007. Palaeogeothermal response and record of late Mesozoic lithospheric thinning in the eastern North China Craton. In: Zhai, M.G., Windley, B.F., Kusky, T.M., Meng, Q.R. (Eds.), Mesozoic Sub-Continental Lithospheric Thinning under Eastern Asia, vol. 280. Geological Society of London (Spec), pp. 267–280.
Huang, T.K., Chi, J.S., 1980. An outline of the tectonic characteristics of China. Continental tectonics 36, 184–197.
Huang, S., Wang, J., 1991. Several heat-flow values from deep drill holes in the northwest depression of the Sichuan Basin, SW China. Chin. Sci. Bull. 36, 47–51.
Huang, J.L., Zhao, D.P., 2006. High-resolution mantle tomography of China and surrounding regions. J. Geophys. Res. 111, 1–21.
Huang, J.L., Zhao, D.P., 2009. Seismic imaging of the crust and upper mantle under Beijing and surrounding regions. Phys. Earth Planet. Inter. 173, 330–348.
Huang, D.F., Liu, B.W., Wang, T.D., Xu, Y.C., Chen, S.J., Zhao, M.J., 1999. Genetic type and maturity of lower Paleozoic marine hydrocarbon gases in the eastern Tarim basin. Chem. Geol. 162, 65–77.
Huang, Z., Li, H., Zheng, Y., et al., 2009. The lithosphere of North China Craton from surface wave tomography[J]. Earth Planet. Sci. Lett. 288 (1), 164–173.
Huang, F., Liu, Q.Y., He, L.J., 2012. Tectono-thermal modeling of the Sichuan Basin since the late Himalayan period. Chin. J. Geophys. 55 (11), 3742–3753.
Irving, A.J., Kuehner, S., Ellsworth, P., 2003. Petrology and thermobarometry of mantle xenoliths from the Eocene Homestead kimberlite pipe, Central Montana, USA. In: 8th International Kimberlite Conference, Victoria, BC, Canada.
Jia, C.Z., Wei, G.Q., 2002. Structural characteristics and petroliferous features of Tarim basin. Chin. Sci. Bull. 47, 1–11.
Jia, C.Z.J., Wei, G.Q., Yao, H.J., 1995. Tectonic Evolution and Regional Structural Geology: Book Series on Petroleum Exploration in the Tarim Basin (in Chinese): Beijing. Petroleum Industry Press (252p).
Jiang, G.Z., Gao, P., Rao, S., Zhang, L.Y., Tang, X.Y., Huang, F., Zhao, P., Pang, Z.H., He, L.J., Hu, S.B., Wang, J.Y., 2016. Compilation of heat flow data in the continental area of China (4th edition). Chin. J. Geophys. 59 (8), 2892–2910.
Jiang, Q., Qiu, N.S., Zhu, C.Q., 2018. Heat flow study of the Emeishan large igneous province region: Implications for the geodynamics of the Emeishan mantle plume. Tectonophysics 724-725, 11–27.
Jiang, G.Z., Hu, S.B., Shi, Y.Z., Zhang, C., Wang, Z.T., Hu, D., 2019. Terrestrial heat flow of continental China: Updated dataset and tectonic implications. Tectonophysics 753, 36–48.
Jin, K.L., 1997. Study on the Organic Petrology: In Case of the Tarim Basin (in Chinese). Seismic Press, Beijing (286p).
Kusky, T.M., Polat, A., 1999. Growth of granite-greenstone terranes at convergent margins, and stabilization of Archean cratons. Tectonophysics 305 (1), 43–73.
Lachenbruch, A., Sass, H., 1977. Heat flow in the United States and the thermal regime of the crust. In: The Earth's Crust, its nature and physical properties, Geophysical Monograph, 20, pp. 626–675.
Laslett, G.M., Green, P.F., Duddy, I.R., Gleadow, A.J.W., 1987. Thermal annealing of fission tracks in apatite, 2.A quantitative analysis. Chem. Geol. 65, 1–13.
Li, Q.Y., 1990. The study on the deep thermal characteristics of Sichuan basin. In: Master thesis of Chengdu Institute of Geology.
Li, G.H., 1992. Terrestrial Heat Flow and Thermal Structure Analysis in Qaidam Basin (in Chinese): Thesis for Master Degree of Institute of Geology. Academia Sinica, Beijing.
Li, P.L., 2003. The Oil and Gas Geology and their Exploration in the Terrestrial Facies Rift-Subsidence Basins. Petroleum Industry Press, Beijing (24–61 (in Chinese).
Li, R.X., Liao, Y.S., 2001. Thermal history of the Permo-Carboniferous Coal Source Rocks in Jiyang Depression, Shengli Oilfield. Acta Geosci. Sin. 22, 85–89 (in Chinese with English abstract).
Li, D.S., Liang, D.G., Jia, C.Z., Wang, G., Wu, Q.Z., He, D.F., 1996. Hydrocarbon accumulations in the Tarim basin, China. AAPG Bulletin 80, 1587–1603.
Li, H.L., Qiu, N.S., Jin, Z.J., 2004. Study on thermal history of Tazhong Area, Tarim basin (in Chinese). Journal of Xi'an Shiyou University 19, 36–39.
Li, H.L., Qiu, N.S., Jin, Z.J., He, Z.L., 2005. Thermal history of Tarim basin (in Chinese). Petroleum Exploration in Western China 1, 15–18.
Li, M.J., Wang, T.G., Chen, J.F., He, F.Q., Yun, L., Akbar, S., Zhang, W.B., 2010. Paleo-heat flow evolution of the Tabei Uplift in Tarim basin, Northwest China. J. Asian Earth Sci. 37, 52–66.
Li, Z.L., Li, Y.Q., Chen, H.L., et al., 2012. Hf isotopic characteristics of the Tarim Permian large igneous province rocks of NW China: implication for the magmatic source and evolution. J. Asian Earth Sci. 49, 191–202.
Li, X., Zhu, P., Kusky, T.M., Gu, Y., Peng, S., Yuan, Y., Fu, J., 2015. Has the Yangtze craton lost its root? A comparison between the North China and Yangtze cratons. Tectonophysics 655, 1–14.
Li, J.W., Li, Z., Qiu, N.S., et al., 2016. Carboniferous-Permian abnormal thermal evolution of the Tarim basin and its implication for deep structure and magmatic activity (in Chinese). Chin. J. Geophys. 59 (9), 3318–3329.
Li, X.L., Liu, S.W., Feng, C.G., 2019. Thermal properties of sedimentary rocks in the Tarim Basin, northwestern China. AAPG Bull. 103 (7), 1605–1624.
Li, X.L., Cai, L., Liu, S.W., et al., 2020a. Thermal Properties of Evaporitic Rocks and their Geothermal Effects on the Kuqa Foreland Basin, Northwest China. Geothermics 88, 101898.
Li, X.J., Gu, Z.Y., Yong, Z.Q., Pan, F., Chen, H., Dong, X., Wu, Q.J., 2020b. Reservoir characteristics, volcanic lithofacies cycles of Emeishan basalt in well Ys1, western Sichuan Basin. Mineral. Petrol. 40 (1), 100–112 (in Chinese with English abstract).
Liu, Q.Y., He, L.J., 2019. Tectono-thermal modeling of the Bohai Bay Basin since the Cenozoic. Chinese Journal of Geophysics-Chinese Edition 62 (1), 219–235.
Liu, S.G., Ma, Y.S., Wang, G.Z., Cai, X.Y., Xu, G.S., Sun, W., 2014. Formation Process and Mechanism of the Sinian-Silurian Natural Gas Reservoirs in the Sichuan Basin. Science Press, China. Beijing China (429p (in Chinese).
Liu, S.W., Lei, X., Wang, L.S., 2015. New heat flow determination in northern Tarim Craton, Northwest China. Geophys. J. Int. 200 (2), 1194–1204.
Liu, S.W., Lei, X., Feng, C.G., Hao, C.Y., 2016. Estimation of subsurface formation temperature in the Tarim Basin, Northwest China: implications for hydrocarbon generation and preservation. Int. J. Earth Sci. 105 (5), 1329–1351.
Liu, Q.Y., He, L.J., Chen, L.C., 2018a. Tectono-thermal modeling of Cenozoic multiple rift episodes in the Bohai Bay Basin, eastern China and its geodynamic implications. Int. J. Earth Sci. 107 (1), 53–69.
Liu, W., Qiu, N.S., Xu, Q.C., Liu, Y.F., 2018b. Precambrian temperature and pressure system of Gaoshiti-Moxi block in the central paleo-uplift of Sichuan Basin, southwest China. Precambrian Res. 313, 91–108.
Liu, Y.C., Qiu, N.S., Li, H.L., Ma, A.L., Chang, J., Jia, J.K., 2020a. Terrestrial heat flow and crustal thermal structure in the northern slope of Tazhong uplift in Tarim Basin. Geothermics 83, 101709.
Liu, Y.C., Qiu, N.S., Chang, J., et al., 2020b. Application of clumped isotope thermometry to thermal evolution of sedimentary basins: a case study of Shuntuoguole area in Tarim Basin. Chin. J. Geophys. 63 (2), 597–611.
Lu, J., Zheng, J., Griffin, W.L., Yu, C., 2013. Petrology and geochemistry of peridotite xenoliths from the Lianshan region: Nature and evolution of lithospheric mantle beneath the lower Yangtze block. Gondwana Res. 23, 161–175.
Lu, J.L., Zuo, Z.X., Shi, Z., Dong, X., Wu, Q.J., Song, X.B., 2019. Characteristics of Permian volcanism in the western Sichuan Basin and its natural gas exploration potential. Nat. Gas Ind. 39 (2), 46–53 (in Chinese with English abstract).

Luo, X., Zhu, C.Q., Zhang, B.S., Tang, B.N., Chen, T.G., 2020. Heat production rate calculation using Gama-ray logging of the sedimentary formation in the Tarim basin. Northwest China. Acta Geoloica Sinica 94 (7), 2078–2088.
Ma, X.H., Li, G.H., Ying, D.L., Zhang, B.J., Li, Y., Dai, X., Fan, Y., Zeng, Y.X., 2019. Distribution and gas-bearing properties of Permian igneous rocks in Sichuan Basin. SW China. Petroleum Exploration and Development 46 (2), 216–225 (in Chinese with English abstract).
Ma, Y.S., Li, M.W., Cai, X.Y., Xu, X.H., Hu, D.F., Qu, S.L., Li, G.S., He, D.F., Xiao, X.M., Zeng, Y.J., Rao, Y., 2020. Mechanisms and exploitation of deep marine petroleum accumulations in China: Advances , technological bottlenecks and basic scientific problems. Oil Gas Geol. 41 (4), 655–683.
Mackenzie, J.M., Canil, D., 1999. Composition and thermal evolution of cratonic mantle beneath the central Archean Slave Province, NWT, Canada. Contributions to Mineralogy and Petrology 134 (4), 313–324.
Mckenzie, D., 1978. Some remarks on the development of sedimentary basins. Earth Planet. Sci. Lett. 40, 25–32.
Menzies, M.A., Fan, W., Zhang, M., 1993. Palaeozoic and Cenozoic lithoprobes and the loss of> 120 km of Archaean lithosphere, Sino-Korean craton, China. London: Geological Society Special Publication 76, 71–81.
Michaut, C., Jaupart, C., Mareschal, J.C., 2009. Thermal evolution of cratonic roots. Lithos 109, 47–60.
Morgan, P., 1985. Crustal radiogenic heat production and the selective survival of ancient continental crust. J. Geophys. Res. 90, 561–570.
Morgan, P., Sass, J.H., 1984. Thermal regime of the continental lithosphere. J. of Geodynamics 1, 143–166.
Mu, S.L., 2009. Exploration Theory, Technology and Practice for Oil and Gas in China's Marine Strata: Beijing. Geological Publishing House (752p).
Neumann, N., Sandiford, M., Foden, J., 2000. Regional geochemistry and continental heat flow: implications for the origin of the south Australian heat flow anomaly. Earth Planet. Sci. Lett. 183 (1–2), 107–120.
Pan, C.C., Zhou, Z.Y., Fan, S.F., 1996. Thermal history of Tarim basin (in Chinese). Bulletin of Mineralogy Petrology and Geochemistry 15, 150–177.
Pan, G.T., Xiao, Q.H., Lu, S.N., Deng, J.F., Feng, Y.M., Zhang, K.X., Zhang, Z.Y., Wang, F. G., Xing, G.F., Hao, G.J., Feng, Y.F., 2009. Subdivision of tectonic units in China. Geol. China 36, 1–28 (in Chinese with English abstract).
Pollack, H.N., 1996. Cratonization and thermal evolution of the mantle. Earth Planet. Sci. Lett. 80, 175–182.
Pollack, N.N., Chapman, D.S., 1977. On the regional variation of heat flow, geothermics and lithosphere thickness. Tectonophysics 38, 279–296.
Pollack, H.N., Hurter, S.J., Johnson, J.R., 1993. Heat flow from the Earth's interior: analysis of the global data set. Rev. Geophys. 31, 267–280.
Qi, L.X., 2016. Oil and gas breakthrough in ultra-deep Ordovician carbonate formations in Shuntuoguole uplift. Tarim Basin. China Petroleum Exploration 21 (3), 38–51.
Qi, J.F., Yang, Q., 2010. Cenozoic structural deformation and dynamic processes of the Bohai Bay basin province, China. Mar. Pet. Geol. 27, 757–771.
Qi, J.F., Lu, K.Z., Zhang, Y.W., 1995. Relationship between the Cenozoic tectonics and oil and gas in the Bohai Bay basin. Journal of China University of Petroleum 19 (Supl), 7–13.
Qiu, N.S., 2002. Characters of thermal conductivity and radiogenic heat production rate in basins of Northwest China (in Chinese): Chinese. J. Geol. 37, 196–206.
Qiu, N.S., Li, S.P., Zeng, J.H., 2004. Thermal history and tectonic-thermal evolution of the Jiyang depression in the Bohai Bay Basin, East China. Acta Geol. Sin. 78, 263–269 (in Chinese with English abstract).
Qiu, N.S., Su, X.G., Li, Z.Y., Liu, Z.Q., Li, Z., 2006. The Cenozoic tectono-thermal evolution of Jiyang depression, Bohai bay basin, East China. Chin. J. Geophys. 49, 1127–1135 (in Chinese with English abstract).
Qiu, N.S., Su, X.G., Li, Z.Y., Zhang, J., Liu, Z.Q., Li, Z., Zhang, L.Y., 2007. The Cenozoic tectono-thermal evolution of depressions along both sides of mid-segment of Tancheng-Lujiang Fault Zone, East China. Chinese J. Geophys. 50, 1497–1507 (in Chinese with English abstract).
Qiu, N., Qin, J., McInnes, B.I.A., Wang, J., Tenger Zhen, L., 2008. Tectonothermal evolution of the northeastern Sichuan basin: constraints from apatite and zircon (U–Th)/He ages and vitrinite data. Geol. J. Chin. Univ. 14, 223–230 (in Chinese with English abstract).
Qiu, N.S., Wei, G., Li, C.C., Zhang, Y., Guo, Y.H., 2009. Distribution features of current geothermal field in the Bohai Sea waters. Oil Gas Geol. 30 (4), 412–419.
Qiu, N.S., Zuo, Y.H., Zhou, X.H., Li, C.C., 2010. Geothermal regime of the Bohai offshore area, Bohai Bay basin, North China. Energy Explor. Exploit. 28, 327–350.
Qiu, N.S., Zuo, Y.H., Chang, J., Li, W.Z., 2014. Geothermal evidence of Mesozoic and Cenozoic lithosphere thinning in the Jiyang sub-basin, Bohai Bay Basin, eastern North China Craton. Gondwana Res. 26 (3–4), 1079–1092.
Qiu, N.S., Xu, W., Zuo, H.Y., Chang, J., 2015. Meso-Cenozoic thermal regime in the Bohai Bay Basin, eastern North China Craton. Int. Geol. Rev. 57 (3), 271–289.
Qiu, N.S., Zuo, Y.H., Xu, W., Li, W.Z., Chang, J., Zhu, C.Q., 2016. Meso-Cenozoic Lithosphere Thinning in the Eastern North China Craton: evidence from thermal history of the Bohai Bay Basin, North China. The Journal of Geology 142, 195–219.
Reiners, P.W., Spell, T.L., Nicolescu, S., Zanetti, K.A., 2004. Zircon (U-Th)/He thermochronometry: He diffusion and comparisons with $^{40}Ar/^{39}Ar$ dating. Geochim. Cosmochim. Acta 68, 1857–1887.
Rosen, O.M., Soloviev, A.V., Zhuraview, D.Z., 2009. Thermal evolution of the northeastern Siberian platform in the light of apatite fission-track dating of the deep drill core. Izvestiya, Physics of the Solid Earth 45 (10), 914–931.
Rudnick, R.L., Mcdonough, W.F., O'Connell, R.J., 1998. Thermal structure, thickness and composition of continental lithosphere. Chem. Geol. 145 (3), 395–411.
Sclater, J.G., Jaupart, C., Galson, D., 1980. The heat flow through oceanic and continental crust and the heat loss of the Earth. Rev. Geophys. 18, 269–311.
Shellnutt, J.G., 2014. The Emeishan large igneous province: a synthesis. Geosci. Front. 5, 369–394.
Shen, X.J., Li, G.H., Wang, J.A., 1994. Terrestrial heat flow and statistical heat flow calculation in Qaidam Basin, Qinghai Province (in Chinese). Acta Geophys. Sin. 37, 56–65.
Sweeney, J.J., Burnham, A.K., 1990. Evaluation of a simple model of vitrinite reflectance based on chemical kinetics. AAPG Bull. 74, 1559–1571.
Tang, Y., Zhang, H., Ying, J., et al., 2013. Widespread refertilization of cratonic and circum-cratonic lithospheric mantle. Earth Sci. Rev. 118, 45–68.
Tang, B.N., Zhu, C.Q., Xu, M., et al., 2019. Thermal conductivity of sedimentary rocks in the Sichuan basin, Southwest China. Energy Exploration & Exploitation 37 (2), 691–720.
Taylor, L.A., Snyder, G.A., Keiler, R., et al., 2003. Petrogenesis of group a eclogites and websterites: evidence from the Obnazhennaya kimberlite, Yakutia. Contributions to Mineralogy and Petrology 145 (4), 424–443.
Tian, K.Q., Yu, Z.H., Feng, M., Yang, C.Y., Liao, Q.J., Zhou, J.S., Sun, X.M., 2000. Eogene Deep Oil and Gas Geology and Exploration in the Bohai Bay Basin. Petroleum Industry Press, Beijing (in Chinese).
Tian, Y., Zhao, D.P., Sun, R.M., Teng, J.W., 2009. Seismic imaging of the crust and upper mantle beneath the North China Craton. Phys. Earth Planet. Inter. 172, 169–182.
Tu, J.Q., 1994. Organic Matter Maturity of Marine Source Rocks and its Paleothermal Conditions of Tarim Basin (in Chinese): Ph. D. Thesis. China University of Mining and Technology, Beijing, China (142p).
Vitorello, I., Pollack, H.N., 1980. On the variation of continental heat flow with age and thermal evolution of continents. J. Geophy. Res. 85, 983–995.
Wang, J.Y., 1996. Geothermics in China. Seismological Press, Beijing, pp. 1–128.
Wang, J.Y., Huang, S.P., 1988. Compilation of heat flow data in the China continental area (in both Chinese and English). Sci. Geol. Sin. 2, 196–204.
Wang, J.Y., Huang, S.P., 1990. Compilation of heat flow data in the China continental area (2nd ed.) (in both Chinese and English). Seismol. Geol. 12, 351–366.
Wang, J., Li, Z., 2001. Sequence Stratigraphy and Evolution of the Neoproterozoic marginal Basins along Southeastern Yangtze Craton, South China. Gondwana Res. 4, 17–26.
Wang, J.Y., Wang, J.A., 1986. Heat flow measurements in Liaohe basin North China. Chin. Sci. Bull. 31, 686–689.
Wang, J.Y., Wang, J.A., 1988. Thermal structure of the crust and upper mantle of the Liaohe Rift Basin, North China. Tectonophysics 145, 293–304.
Wang, J.Y., Wang, J.A., Wang, Y.L., Zhang, Z.Y., 1985. Geothermal measurement in the Liaohe basin. Kexue Tongbao 30 (13), 1008–1010.
Wang, J., Huang, G.S., Huang, S.Y., Wang, J.Y., 1990. Basic Characteristics of the Earth's Temperature Distribution in China (in Chinese). Seismological Press, Beijing.
Wang, J.A., Wang, J.Y., Xiong, L.P., 1992. Geothermal characteristics of the Liaohe Graben and their relationship to oil-gas resources (in Chinese). In: Collected Papers of Geology of Institute, Chinese Academy of Sciences, 5. Science Press, Beijing, pp. 1–77.
Wang, J., Wang, J.A., Shen, J.Y., Qiu, N.A., 1995a. Heat flow in Tarim basin (in Chinese). Earth Sci. 20, 399–404.
Wang, L.S., Li, C., Shi, Y.S., 1995b. The distribution characteristics of heat flow densities in Tarim basin. Science in China 38, 855–856.
Wang, J.Y., Huang, S.P., Chen, M.X., 1996a. Terrestrial heat flux map (in Chinese). In: Yuan, X.C. (Ed.), Geophysical Atlas in China. Geological Publishing House, Beijing, p. 102.
Wang, L.S., Li, C., Yang, C., 1996b. Thermal structure characteristics in the Tarim basin's strata (in Chinese): Chinese J. of. Geophysics 39, 794–803.
Wang, L.S., Liu, S.W., Xiao, W.Y., Li, C., Li, H., Guo, S.P., Liu, B., Luo, Y.H., Cai, D.S., 2002. The characteristics of terrestrial heat flow distribution of the Bohai basin. Chin. Sci. Bull. 47 (2), 151–155.
Wang, F.Y., Zhang, S.C., Zhang, B.M., Xiao, Z.R., Liu, C.W., 2003a. Maturity and its history of Cambrian marine source rocks in the Tarim basin (in Chinese). Geochimica 32, 461–468.
Wang, L.S., Li, C., Liu, S.W., 2003b. Geotemperature gradient distribution of Kuqa foreland basin, North Tarim, China (in Chinese). Chin. J. Geophys. 46, 403–407.
Wang, L.S., Li, C., Liu, S.W., 2005. Terrestrial heat flow distribution in Kuqa foreland basin, Tarim, NW China (in Chinese). Pet. Explor. Dev. 32, 79–83.
Wang, J.A., Wang, Q., Shi, Y.L., Ma, X.F., Zhong, X.M., Li, X.Y., Wang, F.Y., 2015. The cause of ultra-deep-seated oil and gas of Paleogene in Baxian Sag. Nature Gas Geoscience 26 (1), 21–27.
Wei, D.W., 1992. Terrestrial heat flow on the Northern side of Tarim Basin. Sci. Geol. Sin. 1, 93–96.
Wei, X., Xu, Y.G., Feng, Y.X., et al., 2014. Plume-lithosphere interaction in the generation of the Tarim large igneous province, NW China: Geochronological and geochemical constraints. Am. J. Sci. 314 (1), 314–356.
Wu, Q.F., Xie, Y.Z., 1985. Geothermal heat flow in the Song-Liao basin (in Chinese with English abstract). Seismol. Geol. 7, 59–64.
Wu, F.Y., Lin, J.Q., Wilde, S.A., Zhang, X.O., Yang, J.H., 2005a. Nature and significance of the early cretaceous giant igneous event in eastern China. Earth Planet. Sci. Lett. 233, 103–119.
Wu, F.Y., Yang, J.H., Wilde, S.A., Zhang, X.O., 2005b. Geochronology, petrogenesis and tectonic implications of Jurassic granites in the Liaodong Peninsula, NE China. Chem. Geol. 221, 127–156.
Wu, F.Y., Xu, Y.G., Gao, S., Zheng, J.P., 2008. Lithospheric thinning and destruction of the North China Craton. Acta Petrol. Sin. 24 (6), 1145–1174.
Xia, Q.K., Hao, Y.T., Liu, S.C., Gu, X.Y., Feng, M., 2013. Water contents of the Cenozoic lithospheric mantle beneath the western part of the North China Craton: Peridotite xenolith constraints. Gondwana Res. 23, 108–118.

Xiao, X.M., Wilkins, R.W.T., Liu, D.H., Liu, Z.F., Fu, J.M., 2000. Investigation of thermal maturity of lower Palaeozoic hydrocarbon source rocks by means of vitrinite-like maceral reflectance-a Tarim basin case study. Org. Geochem. 31, 1041–1052.
Xiao, H., Ren, Z.L., Cui, J.P., Liao, Y., Han, W., 2008. Relations between geothermal history and hydrocarbon generation in Kongquehe Area (in Chinese). Journal of Northwest University 38, 631–636.
Xie, X.L., Yu, H.J., 1988. The characteristics of the regional geothermal field in Sichuan Basin. J. Chengdu Coll. Geol. 15 (4), 107–114.
Xie, Q.L., Zhou, Z.Y., 2002. Kerogen pyrolysis kinetics simulating experiment used to study low Paleozoic paleotemperature in Tarim basin (in Chinese). Earth Sci. 27, 767–769.
Xiong, L.P., Liu, J., He, L.J., Hu, S.B., Wang, J.Y., 1995. Heat flow and hot spring database in China and compilation of geothermal maps by computer. In: Proc. of the World Geothermal Congress, Florence, pp. 479–483.
Xu, Y.G., He, B., Chung, S.L., Menzies, M.A., Frey, F.A., 2004a. Geologic, geochemical, and geophysical consequences of plume involvement in the Emeishan flood-basalt province. Geology 32, 917.
Xu, W.L., Wang, Q.H., Wang, D.Y., Pei, F.P., Gao, S., 2004b. Processes and mechanism of Mesozoic lithospheric thinning in eastern North China Craton: evidence from Mesozoic igneous rocks and deep-seated xenoliths. Earth Science Frontiers 3, 309–317 (in Chinese with English abstract).
Xu, Z.Z., Chen, S.Y., Wang, Y.S., Zhang, M.J., 2006. Sedimentary characteristics and controlling factors of cretaceous in Jiyang depression. Journal of China University of Petroleum 30, 1–5.
Xu, M., Zhu, C.Q., Tian, Y.T., Rao, S., Hu, S.B., 2011. Borehole temperature logging and characteristics of subsurface temperature in the Sichuan Basin. Chin. J. Geophys. 54 (4), 1052–1060.
Xu, Y.G., Wei, X., Luo, Z.Y., et al., 2014. The early Permian Tarim large igneous province: main characteristics and a plume incubation model. Lithos 204, 20–35.
Xu, Q.C., Qiu, N.S., Liu, W., Shen, A.J., Wang, X.F., 2018. Thermal evolution and maturation of Sinian and Cambrian source rocks in the Central area of the Sichuan Basin, Southwest China. J. Asian Earth Sci. 164, 143–158.
Xu, Q.C., Qiu, N.S., Liu, W., et al., 2019. Reconstructing the basin thermal history with clumped isotope. Chin. Sci. Bull. 64, 566–578.
Yang, X.C., 1985. Discussion on the geothermal field of the Jiyang depression. J. Huadong Petroleum Institute 1, 14–25 (in Chinese with English abstract).
Yang, Y., Wu, F., Wilde, S.A., et al., 2009. In situ perovskite Sr-Nd isotopic constraints on the petrogenesis of the Ordovician Mengyin kimberlites in the North China Craton. Chem. Geol. 264 (1–4), 24–42.
Yang, S.F., Chen, H.L., Li, Z.L., et al., 2013. Early Permian Tarim large igneous province in Northwest China. Science China: Earth Science 56 (12), 2015–2026.
Yang, H.J., Chen, Y.Q., Tian, J., Du, J.H., Zhu, Y.F., Li, H.H., Pan, W.Q., Yang, P.F., Li, Y., An, H.T., 2020. Great discovery and its significance of ultra-deep oil and gas exploration in well Luntan-1 of the Tarim Basin. China Petroleum Exploration 25 (2), 62–72.
Yao, H.F., Ren, Y.L., Shen, B.K., 2006. Reconstruction of the paleogeothermal gradient in the Zhongyuan area, Bohai Bay basin. East China. Earth Science Frontiers 13 (3), 135–140.
Yuan, Y.S., Ma, Y.S., Hu, S.B., Guo, T.L., Fu, X.Y., 2006. Present-day geothermal characteristics in South China. Chin. J. Geophys. 49 (4), 1118–1126.
Zhai, M.G., Santosh, M., 2011. The early Precambrian odyssey of the North China Craton: a synoptic overview. Gondwana Res. 20, 6–25.
Zhai, M.G., Fan, Q.C., Zhang, H.F., Sui, J.L., 2005. Lower crust processes during the lithosphere thinning in eastern China: magma underplating, replacement and delamination. Acta Petrol. Sin. 21, 1509–1526 (in Chinese with English abstract).
Zhang, S., Zheng, Y., 2013. Formation and evolution of Precambrian continental lithosphere in South China. Gondwana Res. 23, 1241–1260.
Zhang, S.C., Wang, F.Y., Zhang, B.M., 2000. Middle-Upper Ordovician source rocks geochemistry of the Tarim basin (in Chinese). Acta Pet. Sin. 21, 23–28.
Zhang, S.C., Zhang, B.M., Wang, F.Y., Liang, D.G., He, Z.H., Zhao, M.J., Bian, L.Z., 2001. The two sets of marine source rocks in Tarim basin: their characteristics of organic matter, depositional environment and controlling factors (in Chinese): Natural. Sci. Prog. 11, 261–268.
Zhang, S.W., Sui, F.G., Lin, H.X., Liu, H., Zhang, S.P., Li, J.Y., 2009. Petroleum Geology and Perspective Evaluation on Pre-Paleogene System in Bohai Bay Basin. Geological Publishing House, Beijing (446p. in Chinese with English abstract).
Zhang, D.Y., Zhang, Z.C., Santosh, M., et al., 2013. Perovskite and baddeleyite from kimberlitic intrusions in the Tarim large igneous province signal the onset of an end-Carboniferous mantle plume. Earth & Planetary Science Letters 361, 238–248.
Zhao, G., Zhai, M., 2013. Lithotectonic elements of Precambrian basement in the North China Craton: Review and tectonic implications. Gondwana Res. 23, 1207–1240.
Zhao, M.J., Wang, Z.M., Pan, W.Q., Liu, S.B., Qin, S.F., Han, J.F., 2008. Lower Palaeozoic source rocks in Manjiaer Sag, Tarim basin (in Chinese). Pet. Explor. Dev. 35, 417–423.
Zhao, L., Zheng, T.Y., Lu, G., 2013. Distinct upper mantle deformation of cratons in response to subduction: constraints from SKS wave splitting measurements in eastern China. Gondwana Res. 23, 39–53.
Zheng, J., Griffin, W.L., O'Reilly, S.Y., et al., 2005. Late Mesozoic-Eocene Mantle Replacement beneath the Eastern North China Craton: evidence from the Paleozoic and Cenozoic Peridotite Xenoliths. Int. Geol. Rev. 47 (5), 457–472.
Zheng, J.P., Griffin, W.L., O'Reilly, S.Y., et al., 2007. Mechanism and timing of lithospheric modification and replacement beneath the eastern North China Craton: Peridotitic xenoliths from the 100 Ma Fuxin basalts and a regional synthesis. Geochim. Cosmochim. Acta 71 (21), 5203–5225.
Zheng, Y., Xiao, W., Zhao, G., 2013. Introduction to tectonics of China. Gondwana Res. 23, 1189–1206.
Zhu, G., Hu, S.Q., Chen, Y., 2008. Evolution of early cretaceous extensional basins in the eastern North China craton and its implication for the craton destruction. Geological Bulletin of China 20, 1594–1604.
Zhu, C.Q., Xu, M., Yuan, Y.S., Zhao, Y., Shan, J.N., He, Z., Tian, Y.T., Hu, S.B., 2010. Palaeogeothermal response and record of the effusing of Emeishan basalts in the Sichuan basin. Chin. Sci. Bull. 55, 949–956.
Zhu, R., Yang, J., Wu, F., 2012. Timing of destruction of the North China Craton. Lithos 149, 51–60.
Zhu, C.Q., Qiu, N.S., Jiang, Q., Hu, S.B., Zhang, S., 2015. Thermal history reconstruction based on multiple paleo-thermal records of the Yazihe area, western Sichuan depression. Chinese Journal of Geophysics-Chinese Edition 58 (10), 3660–3670.
Zhu, C.Q., Hu, S.B., Qiu, N.S., Rao, S., Yuan, Y.S., 2016. Thermal history of the Sichuan Basin, SW China: evidence from deep boreholes. Sci. China Earth Sci. 59 (1), 70–82.
Zhu, C.Q., Hu, S.B., Qiu, N.S., Jiang, Q., Rao, S., Liu, S., 2018. Geothermal constraints on Emeishan mantle plume magmatism: paleotemperature reconstruction of the Sichuan Basin, SW China. Int. J. Earth Sci. 107 (1), 71–88.
Zhu, C.Q., Qiu, N.S., Liu, Y.F., Hu, S.B., 2019. Constraining the denudation process in the Eastern Sichuan Basin using low-temperature thermochronology and vitrinite reflectance data from boreholes. Geol. J. 54, 426–437.
Zuo, Y.H., Qiu, N.S., Zhang, Y., Li, C.C., Li, J.P., Guo, Y.H., Pang, X.Q., 2011. Geothermal regime and hydrocarbon kitchen evolution of the offshore Bohai Bay Basin. North China. AAPG Bulletin 95 (5), 749–769.